12-22-69-20

NASA
SPACE VEHICLE
DESIGN CRITERIA
(ENVIRONMENT)

NASA SP-8023

LUNAR SURFACE MODELS

FOR REFERENCE ONLY

PROPERTY OF MARSHALL LIBRARY

MAY 1969

NATIONAL AERONAUTICS AND SPACE ADMINISTRATION

FOREWORD

NASA experience has indicated a need for uniform criteria for the design of space vehicles. Accordingly, criteria are being developed in the following areas of technology:

Environment
Structures
Guidance and Control
Chemical Propulsion

Individual components of this work will be issued as separate monographs as soon as they are completed. A list of all previously issued monographs in this series can be found on the last page of this document.

These monographs are to be regarded as guides to design and not as NASA requirements, except as may specified in formal project specifications. It is expected, however, that the criteria sections of these documents, revised as experience may indicate to be desirable, eventually will become uniform design requirements for NASA space vehicles.

This monograph was prepared under the cognizance of the Marshall Space Flight Center. An ad hoc committee on Lunar Surface Models, chaired by O. H. Vaughan, Aerospace Environment Division, MSFC, was established to assist in the preparation and review of this monograph. The principal author was R. E. Hutton of TRW Systems; the program coordinators were M. T. Charak of the Office of Advanced Research and Technology, NASA and S. A. Mills of the Goddard Space Flight Center.

The participation and contribution of the following ad hoc committee members are hereby acknowledged:

S. Batterson	NASA, Langley Research Center
H. Benson	NASA, Manned Spacecraft Center
D. Gault	NASA, Ames Research Center
T. Gold	Cornell University
J. O'Keefe	NASA, Goddard Space Flight Center
G. Ulrich	U. S. Geological Survey, Center of Astrogeology
L. Jaffe	Jet Propulsion Laboratory, California Institute of Technology

Valuable contributions were also made by the following individuals:

O. Berg	NASA, Goddard Space Flight Center
N. Costes	NASA, Marshall Space Flight Center
J. Dragg	NASA, Manned Spacecraft Center
J. Harrison	NASA, Marshall Space Flight Center
B. Jones	NASA, Marshall Space Flight Center
H. Moore	USGS, Branch of Astrogeology
R. Pike	USGS, Center of Astrogeology

Comments concerning the technical content of these monographs will be welcomed by the National Aeronautics and Space Administration, Office of Advanced Research and Technology (Code RVA), Washington, D.C. 20546.

May 1969

CONTENTS

1. INTRODUCTION 1

2. STATE OF THE ART 1
   - 2.1 Physical Properties 1
   - 2.2 Morphologic Subdivisions 1
   - 2.3 Topography 2
   - 2.4 Block and Crater Frequencies 4
   - 2.5 Soil Characteristics 4
   - 2.6 Bearing Strength 5
   - 2.7 Density 6
   - 2.8 Soil Layer Thickness 7
   - 2.9 Chemical Composition 7
   - 2.10 Seismic Velocities 7
   - 2.11 Thermal Properties 8
   - 2.12 Optical Properties 9
   - 2.13 Dielectric Constant 10
   - 2.14 Atmospheric Properties 11
   - 2.15 Gravitational Field 11
   - 2.16 Lunar Trafficability 12

3. CRITERIA 13
   - 3.1 Physical Characteristics 13
   - 3.2 Terrain Properties
     - 3.2.1 Mean Slope and Cumulative Frequency Distribution 13
     - 3.2.2 Surface Roughness 13
     - 3.2.3 Topographic Features of Selected Regions 13
   - 3.3 Lunar Craters 14
   - 3.4 Lunar Blocks 23
     - 3.4.1 Block Properties 23
     - 3.4.2 Block Distributions in the Intercrater Region 23
     - 3.4.3 Block Distributions Around Craters 23
     - 3.4.4 Block Fields 23

3.5 Soil Characteristics 27
3.5.1 Soil Parameters 27
3.6 Thermal Properties 30
3.6.1 Brightness Temperature 30
3.6.2 Brightness Temperature Directionality 32
3.6.3 Surface Thermal Properties 34
3.6.4 Thermal Radiation 34
3.7 Electrical Properties 34
3.7.1 Dielectric Constant and Loss Tangent 34
3.8 Optical Properties 36
3.8.1 Normal Albedo 36
3.8.2 Photometric Model 36
3.8.3 Polarization of Moonlight 36
3.9 Lunar Atmosphere 37

REFERENCES 43
APPENDIX A. List of Symbols 49
APPENDIX B. Short Table of Conversion Factors 51
APPENDIX C. Glossary 53
NASA SPACE VEHICLE DESIGN CRITERIA
MONOGRAPHS ISSUED TO DATE 55

LUNAR SURFACE MODELS

1. INTRODUCTION

Engineering models of the lunar surface are needed in mission planning and in the design of landing and exploration vehicles and lunar bases. Models of terrain and soil mechanical properties assist in the evaluation of vehicle landing performance, descent engine plume-surface interactions, and exploration vehicle performance and power requirements. Crater and block (rock) models aid in assessing hazardous landing conditions and obstacles encountered in typical traverse missions. Optical models help in establishing camera design parameters and in determining visual capabilities of astronauts. Dielectric models aid in radar system design. Chemical, bearing strength, density, and thermal models are used in design of surface and sub-surface base structures and surface vehicles.

The lunar surface models presented in this monograph are based on 1968 state of the art; they upgrade and extend the earlier engineering models developed by Vaughan (ref. 1), Vaughan and Costes*, and the criteria guidelines in reference 2. They are founded on a review and interpretation of available literature and lunar data as well as discussions with scientists familiar with data provided by the Ranger, Surveyor, and Orbiter programs, and the Russian Luna probes. In addition, these engineering models reflect, where possible, the consensus of the NASA Lunar Trafficability Model Working Group, composed of members of NASA centers and other government agencies working on lunar exploration programs.

A design criteria monograph being prepared on charged particle radiation also applies to lunar missions. The meteoroid environment is also relevant and is presented in another monograph (NASA SP-8013). Therefore, these environments are not discussed in this monograph.

2. STATE OF THE ART

2.1 Physical Properties

Many physical properties of the Moon have been known for years. The method of their determination and the values presented in this monograph are taken mainly from reference 3. These properties, presented in section 3.1, include the lunar radius, mass density, escape velocity, gravitational acceleration, rotation period, atmospheric density and pressure, and magnetic field strength.

2.2 Morphologic Subdivisions

Two fundamental large-scale morphologic types of lunar terrain are clearly evident—Mare and Upland regions. Well-formed young craters are superimposed on both of these surface types and constitute a widely distributed third basic surface.

*Vaughan, O. H., Jr.; and Costes, N. C.: Lunar Environment: Design Criteria Models for Use In Lunar Surface Mobility Studies, NASA Marshall Space Flight Center, Alabama, Nov. 1968 (unpublished manuscript).

The Mare surface is characterized by relatively gentle topography with low normal albedo and features, such as craters, ridges, rilles, domes, ray systems, and scarps. In contrast, the Uplands have higher albedo, and are rugged with complex superimposed craters.

Besides "Mare" and "Upland," this monograph uses the following more detailed terms; smooth Mare, rough Mare, hummocky Upland, and rough Upland.

Since most lunar regions are composite, the morphologic term applied to any region describes the predominant type of terrain. Hence, a smooth Mare may contain subregions that are rougher than some subregions in a rough Mare.

The topographies of lunar surfaces are characterized by craters of varous sizes and ages. Ideally, the surfaces can be grouped into two types*: (1) the young surface where the frequency distribution directly reflects the rate of crater production, and (2) the "steady state" surface which is the result of the combined effects of crater production and erosion-infilling produced by extensive cratering (crater saturation). Crater frequencies can be expressed approximately by equations of the form $N_o = K D^n$ where N_o is the cumulative number of craters per unit area greater than diameter D, and K and n are constants.The exponent, n, is about -3 for the young surface in which the craters are fresh and uneroded. For the "steady-state" surface (ranging from fresh, well-preserved craters to those so eroded and filled that they are barely discernible), the exponent, n, is about -2 and the coefficient K is 10^{-1}.

2.3 Topography

Rowan and McCauley (refs. 4 and 5) demonstrated with Earth-based photography that the median slope was related to the slope length** for both terrestrial and Mare topography (a linear relation on a log-log plot). The relationship thus obtained from Earth-based lunar observations predicted the mean slope which was later measured from Ranger 7 photographs (when the 0.75 km resolution was extrapolated to one meter). With Orbiter data, R. J. Pike*** extended the work of Rowan and McCauley and developed relations between the mean lunar slope and slope length for the smooth Mare, rough Mare, hummocky Upland, and rough Upland.

*Moore, H. J., "Some Observations of the Lunar Trafficability Problem," U. S. Geological Survey, Nov. 1968 (working paper).

**The slope length is the incremental horizontal distance between two elevations over which the slope is to be determined. It is also referred to as sample cell length by Rowan and McCauley.

***Pike, R. J., "Preliminary Models of Slope Distributions on the Moon," U. S. Geological Survey, Branch of Astrogeologic Studies, Oct. 29, 1968 (working paper).

In addition, Pike's study of terrestrial slope distributions indicated identical cumulative distributions when normalized to the mean slope, regardless of the gentleness or steepness of the mean slope. By assuming that lunar slopes have the same characteristic distributions, Pike developed a basic distribution model using photoclinometry data obtained from 7 lunar regions (data read to 0.6 meter resolution, but most likely are valid only above 1 meter). The slope distribution model presented herein, is a current estimate from a continuing investigation by Pike and others at the Center of Astrogeology, U. S. Geological Survey.

Lunar topography studies are also being conducted by the Mapping Sciences Laboratory at the NASA Manned Spacecraft Center (MSC) in support of the Apollo program, primarily for the landing sites in the Mare regions. Cumulative slope distributions are presented* for slope lengths of about 1 and 10 meters for various locations in the Mare region. The data demonstrate that the slope distributions, for a single slope length, vary from site to site, even though, within the context of the morphological subdivisions, the region might be termed a smooth Mare region. Therefore, within a given morphologic region, a distribution exists for the mean lunar slope for any single slope length. The nominal lunar surface model presented in this monograph provides an estimate of the most likely value of the mean slope for a given slope length.

Variations in the distribution of the average slope for a single base length can be inferred from data in reference 4 and unpublished MSC data (private communication). These MSC data consisted of about 50 lunar slope cumulative frequency distributions for Apollo landing site II P-8 in Sinus Medii. From the data the mean slope and standard deviation were computed to be 4.5° and 1.2°, respectively for the lunar module base length of about 8.5 meters (distance between foot pads). These results were used in establishing the relation between slope standard deviation and mean slope.

The United States Air Force Aeronautical Chart and Information Center also uses photometric techniques to determine lunar topography. Topographic charts included in reference 6 show 1 meter contour lines for Lunar Orbiter site II S-2.

The lunar surface roughness models are described in terms of power spectral density (PSD) and were derived from data obtained from Pike (USGS) and Rozema (ref. 7). Similar data have been obtained by the NASA Manned Spacecraft Center although its interest has been concerned primarily with the smooth Mare regions in the Apollo belt. In reference 8, Jaeger and Schuring present power spectral density data for the Mare Cognitum. They also present a procedure that utilizes PSD data to determine the dynamic response of a vehicle moving over the lunar surface.

According to Pike's data, the Mare regions contain both the smoothest and roughest regions on the Moon with the Upland roughness falling in between two extremes. Even though the Mare has rougher regions than the Uplands, the steepest slopes are found in the Upland

*Anon.: "A Preliminary Analysis of Photometric/Computer Terrain Data for Lunar Trafficability Models," Mapping Sciences Laboratory, NASA Manned Spacecraft Center, Oct. 4, 1968 (working paper).

regions. Table I summarizes the relations between the minimum, nominal, and maximum PSD models of lunar surface roughness presented in this monograph and the corresponding morphologic classifications used in references 1 and 4 and those adopted herein.

TABLE I

LUNAR SURFACE PSD MODELS AND MORPHOLOGIC CLASSIFICATIONS

Lunar Surface PSD Models	Morphologic Classification		
	This Monograph	Reference 1	Reference 4
Minimum	smooth Mare	dark regional Mare	smooth Mare
Nominal	rough Upland/ hummocky Upland	smooth regional Mare; smooth rayed Mare	Upland
Maximum	rough Mare	rough rayed Mare	rough Mare

2.4 Block and Crater Frequencies

Most of the block (protuberance) and crater data models given in this monograph were derived from data furnished by H. J. Moore. These models also included results obtained by E. Shoemaker and E. Morris of USGS and R. Choate of JPL. Often the block counts by various investigators differed substantially, probably because different lunar regions and different sizes were used in making the counts. Block frequency data in this monograph reflect a compromise between the two block frequency curves in reference 9 (figs. III-42 and IV-34). The workers mentioned earlier are continuing their block frequency investigations, and the final differences between their frequency distributions should be resolved in the near future.

2.5 Soil Characteristics

Cameras on the Surveyor spacecraft with about 1 mm resolution (refs. 9 to 14) and Luna spacecraft with a resolution of several mm (ref. 15) have provided detailed information on the lunar surface material in both Mare and Upland regions. Surveyors 1 and 3 and Lunas 9 and 13 landed in a rough Mare region (Oceanus Procellarum, Western limb), Surveyor 5 landed in a smooth Mare region (Mare Tranquillitatis, Eastern limb), Surveyor 6 landed

between the rough and smooth Mare regions (Sinus Medii, middle region), and Surveyor 7 landed in the Uplands near Tycho. Data from both U. S. and U.S.S.R. spacecraft indicate the surface material to be a matrix of fine, partially cohesive particles less than 1 mm in diameter with a few rocks scattered in and on the matrix. Cherkasov et al. (ref. 16) concluded that at the Luna 13 landing site the lunar surface seems to be a layer of granular, loose, weakly-cemented material consisting of grains and granules of porous mineral which are weakly interconnected at contact points. A terrestrial analog of this lunar material was described by the Russian investigators as a lightly-cemented sand with the addition of larger particles while Scott describes it as having properties of a slightly moist beach sand. In this monograph the surface material is simply called a "soil". Other sources often call the surface material the regolith or epilith.

2.6 Bearing Strength

The soil bearing strength, according to reference 14, varies rapidly in the first few mm of depth. For the first 1 mm of depth, the bearing strength is less than 0.1 N/cm^2 (0.1 $newtons/cm^2$), based on the imprints of small rolling fragments. From 1 to 2 mm the bearing strength increases to 0.2 N/cm^2, based on the imprint made by the alpha scattering experiment sensor head. Based on penetrations of the crushable blocks located on the underside of the Surveyor spacecraft truss frame, the bearing strength at a depth of 2 cm was estimated to be 1.8 N/cm^2. The analysis of the Surveyor 1 landing indicates the bearing strength to be between 4.2 and 5.5 N/cm^2 at a depth of about 5 cm. The bearing capacity was also estimated from data obtained on Luna 13. This spacecraft (refs. 15 and 16) carried a conical shaped penetrometer (103° cone, maximum diameter of 35 mm) which was forced into the soil by the thrust force developed by a small solid fuel jet engine (thrust of 6.5 kg for 0.8 seconds). The bearing capacity is listed as 0.68 kg/cm^2 (or 6.67 N/cm^2) at about a 4 cm depth, a little larger value than the estimates made from Surveyor data. In the same Russian references the soil cohesion is estimated to be 0.005 kg/cm^2 (0.049 N/cm^2) or essentially the same as the mean value estimated from Surveyor data.

Reference 17 lists a value of 0.18 kg/cm^3 (1.8 $N/cm^2/cm$) for a parameter called the coefficient of proportionality between the intensity of load and the penetration depth. According to data obtained by Scott with the soil mechanics surface sampler (SMSS) on Surveyor 7 (ref. 14), the force exerted on the closed scoop was 27 N at a penetration depth of about 3 cm. With a closed scoop area of about 12.5 cm^2 the ratio of the average pressure to the penetration depth is 0.72 $N/cm^2/cm$, roughly one-half the value estimated from Luna 13 data. Test method differences may explain the divergence in this value. The Surveyor 7 test was static while the Luna 13 test was dynamic; also the penetrator sizes and shapes were different.

Jaffe (ref. 18) presents a plot of Surveyor bearing capacity data against penetration depth for various bearing width to depth ratios. The width to depth ratios extended from 0.8 to 1.0 and from 5 to 10. These data appear to have approximately a linear relation whose slope ranges from about 0.8 to 1.1 $N/cm^2/cm$.

Bearing pressure tests made with the surface sampler on Surveyors 3 and 7 indicated the soil deformations were characteristic of the general shear type of failure described in reference 19. When the 2.54 cm wide (closed scoop) surface sampler was forced into the lunar soil to a depth of 1.27 cm, the adjacent surface bulged upward and cracked to a distance of 13 to 15 cm from the edge of the sampler (ref. 20).

2.7 Density

On the basis of radio telescope and radar data, Matveev et al. (ref. 21) concluded the soil density increased by a factor of 1.5 to 2 within about the first 4 cm and then remained essentially constant to a depth of 1 to 2 m; at a depth of about 7 to 15 m the density apparently increases sharply to the density of solid rock. One of their density models assumed a density of 0.6 gm/cm^3 on the surface, increasing to 1 gm/cm^3 at a depth of about 4 cm. The other model assumed a density of 1 gm/cm^3 on the surface which increased to 1.6 gm/cm^3 at a depth of about 4 cm. However, they did not believe the data to be sufficient to determine which density model was most probable. Tikhonova et al. (ref. 22) used two different, three-layer soil models as well as thermal radiation data in studies to determine the reflection coefficient. A surface density of 0.7 gm/cm^3 which increased to 2.5 gm/cm^3 at depths greater than about 100 cm was assumed in both models. Jones (ref. 23) recently proposed a density-depth model for the outermost lunar layer. He considers this layer to be composed of particles of approximately the same size and the increase in density to be the result of increasing compaction with increasing depth.

Comparison of bearing test data obtained by Surveyor spacecraft on the Moon and similar tests on Earth lead Scott (ref. 20) to conclude that the soil density was between 1.5 and 2.0 gm/cm^3 with a porosity from 0.35 to 0.45. Scott states that if a low density surface layer exists, it can have a thickness of 1 or 2 mm at most. Comparison of the observed landing dynamic behavior on Surveyor spacecraft with theoretical predictions using soil densities between 1 and 2 gm/cm^3 were in approximate agreement.

Cherkasov and Shvarev (ref. 17) show a comparison of various properties of the soil layer from data obtained from Luna 13 and Surveyors 1 and 3. The comparison includes soil structure, density, cohesion, internal friction angle, variation of bearing stress with penetration, bearing capacity, minimum soil layer thickness, and analogy with terrestrial soil.

The overall conclusion from the Surveyor data is that the soil is strikingly similar at all five sites. However, the thickness of this soil layer appears to vary from one morphologic region to another and within the same morphologic region.

2.8 Soil Layer Thickness

Estimates of the thickness of the soil layer are made from geometrical characteristics of observed craters. Gault et al. (ref. 24) observed from laboratory cratering studies that impacts against targets of fragmental materials overlying a rock substrate could produce craters with a peculiar concentric or terraced structure. When the fragmental material layer was sufficiently thick and the substrate did not interfere with the crater growth, a normal bowl-shaped crater was found. Oberbeck and Quaide (refs. 25 and 26) developed analytical relations between characteristic crater shapes and the fragmental surface layer thickness. Using these relations and Orbiter data, they estimated the soil-like layer thickness at various locations on the lunar surface. Their results indicated that the typical soil layer could range from 1 to 20 meters. However, T. Gold of Cornell University (personal communication) believes that there may be no interface in many regions and that the soil becomes firmer and more dense as one goes deeper. Scott (ref. 9), on the basis of SMSS operations on an Upland site (Surveyor 7), stated that the thickness of the soil layer ranged from 1 cm to at least 15 cm over the operational area. The lower estimate of thickness resulted from encounters with sub-surface obstructions through which the SMSS could not excavate. The encounters may have been with the top of the rock substrate or a local larger block. In any event, the existence of larger areas in which the soil layer is only a few centimeters thick is unlikely.

2.9 Chemical Composition

Estimates of the chemical composition of the soil are based on data returned from the alpha scattering instruments on Surveyors 5, 6, and 7. The most common elements are oxygen, silicon, and aluminum (as on Earth), with atomic percentages of about 60, 20, and 7 percent, respectively (ref. 9). This chemical composition is similar to a terrestrial basalt and/or a meteoritic basaltic achondrite material. The Uplands have a 2 percent iron content on the basis of one sample, and the Maria have a 5 percent iron content on the basis of four samples. This difference may account for the lighter color of the Uplands in some areas. Laboratory calibration data indicated that the amount of lunar material which adhered to the magnets is consistent with a basaltic material rather than with an acidic or ultrabasic material and that content of fine-grained magnetic particles is less than ¼ percent by volume.

2.10 Seismic Velocities

Preliminary estimates of the seismic velocities were made from analysis of the Surveyor landing leg strain-gage data recorded during landings and during vernier engine firing tests. These estimates were based on observations of the low spacecraft amplitude oscillations seen in the strain-gage readings at the end of the transient record (which were lower than the oscillations measured while on a rigid surface). This frequency shift information was used in

conjunction with elasticity theory and assumed ranges of Poisson's ratio to estimate shear and compressional wave velocities in the soil. These values are about an order of magnitude lower than a typical Earth soil in situ. More extensive analysis of these strain-gage data and Earth-based test data is being conducted for JPL by G. Sutton of the University of Hawaii. Results of his study indicate that the seismic speeds may be somewhat higher than the preliminary estimates presented in reference 14 as well as the "frame speed" (the seismic speed in a granular material when the pore-filler material is removed) measured in a porous granular material (ref. 27).

2.11 Thermal Properties

Infrared (10-12 microns) and photometric (0.45 microns) measurements were made by Saari and Shorthill from Earth-based observations; their results are presented in the form of isothermal and isophotic charts for 23 phase angles (ref. 28). The infrared temperatures as measured are not independent of the observation angle (as they are for a Lambertian surface), but have a directional effect; references 29 and 30 point out these directional characteristics as one of the most anomalous characteristics of the surface. Montgomery et al. (ref. 31) concluded the directionality effects are caused by roughness of the surface. A mathematical expression relating infrared temperature to incident and observational directions has been developed from experimental data by Ashby and Burkhard (ref. 32).

Calvert (ref. 33) fitted a Fourier series to the equatorial brightness temperature measurements of Murray and Wildey (ref. 30), Low (ref. 34), and Sinton (ref. 35) over a complete lunation and presented the coefficients through the fiftieth order. Surface temperature anomalies* for local regions much hotter or cooler than the surrounding regions have been detected and closely examined by Shorthill and Saari (ref. 28). The brightness temperature differs from the actual surface temperature in three ways. First, the lunar surface is assumed to be a black body. Second, the thermal radiation is measured only over the 10- to 12-micron portion of the infrared band. Third, the thermal energy measured by the detector is an average of the radiation from distribution of temperatures over a region of the Moon's surface. The size of the region changes with the location being viewed. The region is a circular area from 14 to 17 km in diameter when viewed at the center of the Moon's disk. The Planck radiation equation is then used with the 10- to 12-micron band radiation and corrected for atmospheric absorption to determine the brightness temperature. The derived brightness temperature and actual surface temperature can be regarded as approximately equal.

An attempt to determine effective constant material thermal properties for the Maria and Uplands with Earth-based measurements has been unsuccessful (ref. 36) because variations within a region (Maria or Upland) are as great as the average variation between regions. For this reason, the lunation cooling curves derived from experimental infrared measurements taken from Earth are not uniquely determined, but may be combined statistically to obtain an average cooling curve.

*Over 400 anomalies have been recorded. Mare Humoram typically showed 10°K enhancement above the surrounding Uplands.

Surveyor spacecraft instrument compartment temperature data have been used to infer values of the soil thermal inertia, $\gamma = (k\rho c)^{-1/2}$, where k is thermal conductivity, ρ is density, and c is specific heat. The Surveyor data indicated a constant γ can not adequately represent Earth-based measurements during both eclipse and post-sunset. Winter and Saari (ref. 37) recently developed a particulate lunar soil model which agrees with both eclipse and post-sunset cooling. Surveyor data (ref. 14) indicated a value of γ of about 800 agreed best with the equatorial landing sites. Eclipse data, which give an estimate of γ for the insulating surface material, indicate a value for γ of about 1100 to 1400. Figure IV-14 in reference 14 shows the directionality effect at a sun angle of 60 degrees.

2.12 Optical Properties

A review of the history of lunar photometry is presented by Minnaert (ref. 38). Basic visual and photometric quantities are discussed by Ziedman (ref. 39) who also gives analytical procedures for assessing detection of lunar surface obstacles.

The parameter commonly used to express the diffuse reflectivity of the full Moon is called the normal albedo. Published albedo values for various lunar surface features are not entirely in agreement. Errors in determining the normal albedo, for example, may arise because of uncertainty in the photometric function, extrapolations to zero phase angle, luminescence, and limitations or errors in recording and measuring instruments. Early measurements of normal albedo values are presented in references 38, 40, and 41. Reference 42 gives more recent measurements of normal albedo for more than 300 lunar surface locations, comparable to those published earlier but not including the brightness surge effect at zero phase. Reference 43 lists normal albedo values after an extrapolation to zero phase, which take into account the brightness surge effect. These investigators state that the brightness-phase relations show a nonlinear surge close to zero phase and that the brightness may increase by as much as a factor of 2 from ±5° to 0° phase angle. For example, they give the average Mare and Upland normal albedos as 0.13 and 0.27, respectively. In contrast to these, Minnaert (ref. 38), while quoting Sytinskaya's data, gives the normal albedo as 0.065 and 0.105 for the Mare and Upland regions, respectively.

Pohn and Wildey (ref. 44) obtained other normal albedo data by using a combined photographic and photoelectric technique with improved photo processing methods. The albedo measurements indicated on the photoelectric-photographic map of the normal albedo of the Moon in reference 44 appear to be higher than those in references 38, 40, 41, and 42 but lower than those in reference 43. (Pohn and Wildey stated in a private communication that their albedo measurements included the surge effect.) Gehrels et al. (ref. 43) give the normal albedo of Mare Crisium as 0.082 to 0.092 in the ultraviolet region (3600 Å), 0.194 to 0.218 in the infrared region (9400 Å), and 0.08 to 0.15 over the visible region (3800 to 7800 Å).

Preliminary estimates of the average normal albedo values for the back side of the Moon have been made by J. Dragg of NASA, MSC (personal communication) from Orbiter photographs. He indicates the average normal albedo to be 0.217 for the back side of the Moon.

For different areas of the Moon, there are variations in the photometric function. This function relates the brightness of the lunar surface to the viewing angle and solar incidence angle. Two basic photometric functions (based on different assumptions) have been derived from Earth-based observations. The first was derived by Hapke (ref. 45) by fitting data to a theorectical scattering model of the lunar surface. The model was later revised in 1966 (ref. 46). The second, based entirely on Fedoretz' lunar photographic data (ref. 47), was derived empirically by Herriman, Washburn, and Willingham in 1963 (ref. 48). Since the data exhibited a large data scatter for small phase angles, Willingham developed a revised model with data from Sytinskaya and Sharanov in 1964 (ref. 49). These four photometric functions are compared by Watson in reference 50. Efforts are presently in progress to develop a more accurate photometric function. The function presented herein is that developed in reference 47 and is commonly called the Fedoretz function.

2.13 Dielectric Constant

The dielectric constant of lunar material has been estimated from the reflection at the surface of microwave emission and from radar return data. Radar observations and observations of the natural radio emission of the Moon led Matveev (ref. 21) to conclude that the most probable values for the effective dielectric constant were 1.7 at a 3 cm wavelength, 2.25 averaged over the wavelength range 0.8 to 12 cm, and 3.2 averaged over the wavelength range 33 to 784 cm.

Earth-based data obtained by Thompson (ref. 51) indicated the dielectric constant in the Uplands is about twice that in the Mare. On the basis of Explorer 35 data obtained near the Moon, Tyler (refs. 52 and 53) has estimated the effective dielectric constant to be 3.2 in the Mare and 2.8 in the Uplands at a 2.2 meter wavelength at depths of about 25 cm to a depth of many meters. Later, on the basis of radar return data from the Surveyor spacecraft at a 2 to 3 cm wavelength (appropriate for surface estimates), Muhleman (ref. 14) estimated the surface dielectric constant to be from 1.84 to 2.47 in the Mare (Surveyors 1, 3, 5, and 6) and from 2.88 to 3.68 in the Upland (Surveyor 7).

Estimates of the dielectric constant by Russian investigators (refs. 22 and 54) do not differentiate between Mare and Upland regions. In reference 54, the dielectric constant estimate is about 3 at a 1.7 m wavelength. In reference 22, the dielectric constant is expressed as a function of wavelength and soil density. For a soil density of 1.5 to 2.5 gm/cm^3, the corresponding dielectric constant lies in the range 2 to 3 at the Surveyor wavelength (2 to 3 cm) and in the range 3 to 4.9 at the Explorer wavelength (2.2 m). Additional laboratory measurements of dielectric and loss tangent values on various

terrestrial soils and rocks are given in references 55 and 56; earlier lunar measurements are presented in reference 33. Other data for the electrical properties of rocks can be found in a recent paper by Campbell and Ulrichs.*

2.14 Atmospheric Properties

There is general agreement that the Moon has essentially no atmosphere (ref. 3). One of the early estimates of atmospheric density was made by Dollfus (given in ref. 3) from a study of the polarization of light from the Moon which led to an upper bound density estimate of 10^{-9} times a standard Earth sea level density. Later Elsmore (also ref. 3) observed the bending of radio waves from Crab Nebula as they passed close by the Moon. From these data, it was estimated that the electron density was from 10^3 to 10^4 electrons/cm^3 which is consistent with a lunar atmospheric density of 10^{-13} times that of Earth.

Data obtained from Luna 10 (ref. 57) indicates the ion density is less than 100/cm^3. On this basis an estimate of the lunar atmospheric density is 10^{-15} times that of Earth.

Gold (personal communication) has suggested that the moon may possess an atmosphere of photoelectrons close to the surface and that this type atmosphere may provide a mechanism for discharging electrical effects.

2.15 Gravitational Field

In reference 58, the variation of the lunar gravity field is given in terms of selenographic latitude and longitude. At zero latitude and longitude, the value is 1.623 m/sec^2 which can vary by as much as 0.06 percent with latitude and longitude. Urey (ref. 59) discusses the gravitational anomalies detected by Muller and Sjogren (ref. 60), which are believed to be caused by local, high density masses inside the Moon (mascons). These high density or mass concentrations (located in circular maria) were noted because Orbiter spacecraft velocities increased as the vehicles passed over certain lunar depressions. Normally, the spacecraft velocity would decrease since there should be a mass deficiency with respect to the surrounding terrain. The locations of anomalies of this type are important to a landing spacecraft as mascons could cause a trajectory perturbation and thus a potential miss of an assigned landing point. Urey estimates the anomalies to be 750 milligals (0.00750 m/sec^2) at the nominal lunar surface. This anomaly corresponds to about 0.5 percent of the nominal gravity field, and therefore about an order of magnitude larger than the variation with latitude and longitude. Tolson and Gapcynski (ref. 61) expressed the gravity potential in the usual series of spherical harmonics and determined a set of coefficients through degree and order five from Orbiter 1, 3 and 4 data.

*Campbell, M. J.; and Ulrichs, U.: The Electrical Properties of Rocks and their Significance for Lunar Radar Observations. Working paper submitted to Journal of Geophysical Research.

2.16 Lunar Trafficability

One of the important problems in designing for or predicting vehicle mobility over lunar terrain involves consideration of the soil and vehicle interaction. Currently, designers of lunar roving vehicles have had to rely on approaches developed to predict terrestrial off-road performance capability or trafficability. A recent survey by Cornell Aeronautical Laboratories of the state of the art in terrestrial off-the-road locomotion (ref. 62) concluded that there were two general approaches to assessing off-road mobility performance of wheel and track vehicles: one theory initially developed by Bekker (refs. 63 and 64) and modified by personnel at the Land Locomotion Laboratory (LLL), Army Tank Automotive Center; the other theory developed by the U. S. Army Engineering Waterways Experiment Station (WES). The latter approach gives a "go" or "no-go" prediction from an interpretation of cone penetrometer tests in a soil along with empirical formulas; it is primarily applicable to quick predictions of the trafficability of fine-grained soils and sands. Being based on historical performance data of conventional vehicle designs, both methods have limited use for new and different vehicles incorporating unconventional design concepts for operation in a lunar environment.

The Bekker method examines mobility from a more fundamental viewpoint to obtain performance predictions and thrust requirements. The procedure assumes a combined frictional-cohesive soil and then develops wheel-soil equations describing wheel sinkage and tractive force (soil thrust). The relations involve several semi-empirical moduli for the soil. The Cornell survey (ref. 62) mentions that there is no comparable work to match the Bekker-LLL approach in depth. Also, when it is applied with judgment to real problems, it often yields reasonable results. However, one major shortcoming of the Bekker-LLL theory is that it was only developed for mobility over flat terrains. Peters (ref. 65) examines the forces at the wheel-soil interface, and the corresponding soil failure modes, in an attempt to relate kinematic, force, and energy parameters.

Soil cohesion is another factor affecting the mobility of a vehicle operating on the lunar surface. Halajean (ref. 66) considers the influence of cohesion and gravity field on vehicle performance on level terrain. His results show cohesion has a negligible influence in low cohesive soils compared to the soil frictional contributions in Earth's gravity field. However, in a lunar gravity field the relative importance of cohesion is much greater.

Soil cohesion takes an added importance in assessing vehicle performance on slopes (ref. 67). At high slope angles (approaching the angle of soil repose), the soil's strength and rigidity because of its frictional character tend to disappear, leaving mainly the cohesive component for load support. Karafiath and Nowatski (ref. 68) used a modified version of Terzaghi's bearing capacity theory to determine the influence of a sloping surface on the reduction in bearing capacity. Their results can be used to better define the lunar soil and vehicle interaction with respect to the slope and soil loading geometry.

Soil adhesion is an additional factor affecting the design and mobility of a lunar roving vehicle. The clogging of soil on wheels and tracks and the entrance of the soil into bearings that are not completely enclosed could cause problems in the lunar vacuum environment.

3. CRITERIA

The lunar surface models and related physical, chemical, thermal, and mechanical properties presented here should be used in mission analyses and in design of landing and exploration vehicles and lunar bases.

3.1 Physical Characteteristics

Table II gives the geophysical and astronomical data (ref. 3) to be used for lunar missions.

3.2 Terrain Properties

3.2.1 Mean Slope and Cumulative Frequency Distribution

Figure 1 shows the mean lunar slope, $\overline{a}$, for various slope lengths, ΔL. The nominal curve is representative of the rough Upland and hummocky Upland regions. The minimum curve is representative of a smooth Mare while the maximum curve is representative of the rough Mare. The standard deviation of the mean slope distribution for a single slope length is approximately 0.3 times the mean slope.

The cumulative distribution of slope per unit mean slope is shown in figure 2, while figure 3 shows cumulative distributions for various mean lunar slopes.

3.2.2 Surface Roughness

Figure 4 presents lunar surface roughness in terms of power spectral density (meters^2/cycle/meter). Representative data for very smooth and very rough terrestrial terrains are also shown for comparison.

3.2.3 Topographic Features of Selected Regions

Table III presents data on lunar surface features which are representative of large-scale slopes and should be considered in the design of lunar roving vehicles.

3.3 Lunar Craters

Table IV illustrates idealized crater shapes with depth and rim height data for various age groups. Figure 5 shows the cumulative crater frequency distribution for the "steady-state" surface for various age groups. The lower line indicates the cumulative frequency for only fresh craters. The next higher line indicates the cumulative frequency for both fresh and young craters. The highest line shows the frequency for all crater types. The figure also indicates the percent of original relief remaining for each age group. Figure 6 shows the range of crater cumulative frequency distributions for the smooth Mare, rough Mare, and Upland terrains as discussed in this monograph.

TABLE II

LUNAR PHYSICAL VALUES

Parameter	Value
Radius (km)	1738.0
Mass (gm)	7.35×10^{25}
Density (gm/cm^3)	3.34
Gravitational acceleration (m/sec^2)	1.62
Escape velocity (km/sec)	2.38
Sidereal period, true period of rotation and revolution (days)	27.322
Synodic period, new Moon to new Moon, (days)	29.531
Atmospheric pressure (Estimated)	$<10^{-15}$ Earth's at sea-level
Atmospheric density (Estimated)	$<10^{-15}$ Earth's at sea-level
Magnetic field strength (Estimated)	<10 gamma at surface

TABLE III

LARGE-SCALE SLOPES AND OTHER DATA FOR LUNAR FEATURES*

Harbinger Mountains Local Slopes on Rille Wall, 39° Long Slopes of Rille Wall, 22° Long Slope on Upland Ridge, 13° to 19° Relief of Ridges, 200 to 400 m Slopes on Small Rille Walls, 15° Relief of Small Rilles, 200 to 400 m
Schröters Valley Long Slope of Rille Wall, 31° for 1 km Relief, 663 m
Near Aristarchus (Slope of Upper to Lower Plateau) Long Slope, 22.5° for 3 km
Small Crater (180 m diam) in Schröters Valley Relief, 26 m Slopes of Upper Walls near 29° to 31°
Domical Hill Width of Crest, 4 km Typical Relief 850 meters Drop in 2.5 km 850 meters Rise in 3.5 km Comment-Most hills are hummocky at 1 to 10 meter wavelengths and many of the dome-type features and ridges and/or rills will be strewn with block fields and small craters with blocky ejecta.

*Moore, H.J., "Some Observations of the Lunar Trafficability Problem," U.S. Geological Survey Nov. 1968 (working paper).

TABLE IV

IDEALIZED CRATER SHAPES IN RELATION TO THEIR MORPHOLOGY*

Crater Type	Typical Profile	Depth to Diam Ratio	Rim Height to Diam Ratio
Fresh	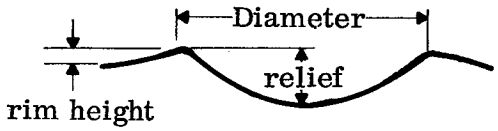	0.23 to 0.25	0.022 to 0.06
Young		0.17 to 0.19	0.016 to 0.045
Mature		0.11 to 0.13	0.008 to 0.03
Old			

*Moore, H. J., "Some Observations of the Lunar Trafficability Problem," U.S. Geological Survey Nov. 1968 (working paper).

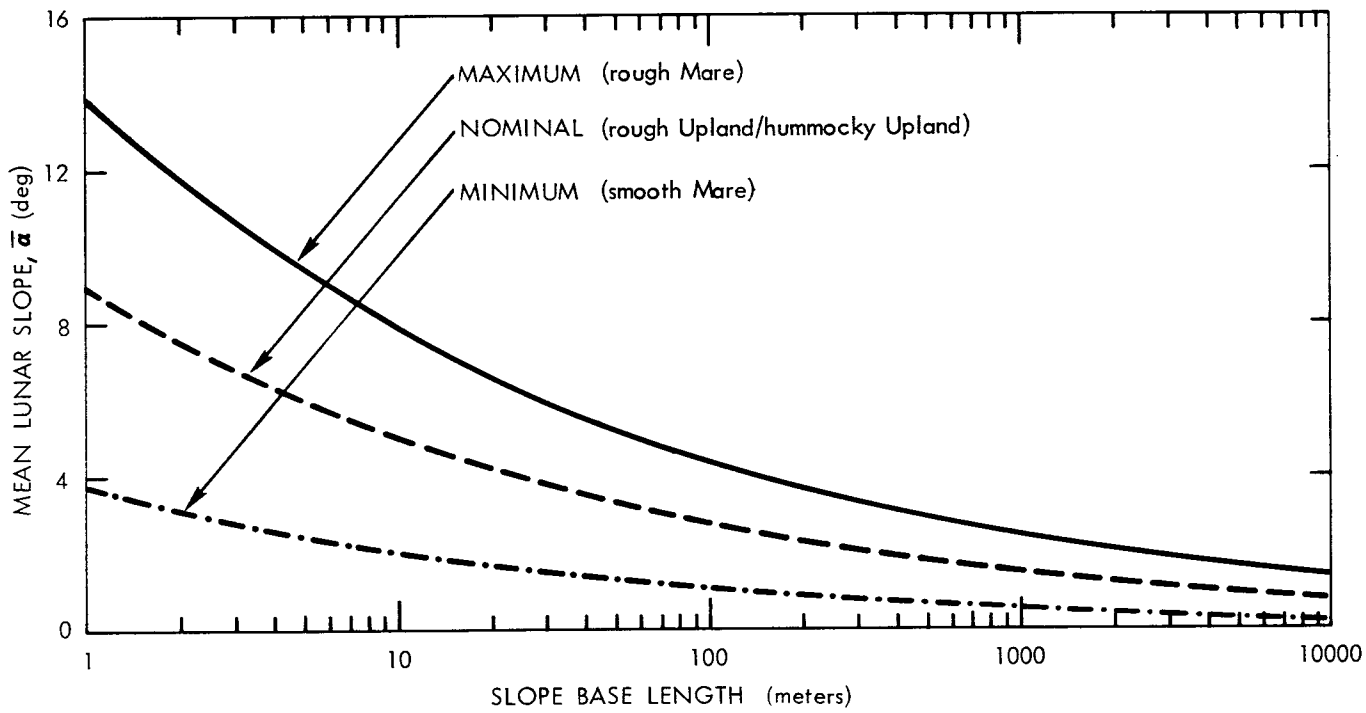

Figure 1. - Variation of mean lunar slope with slope length.

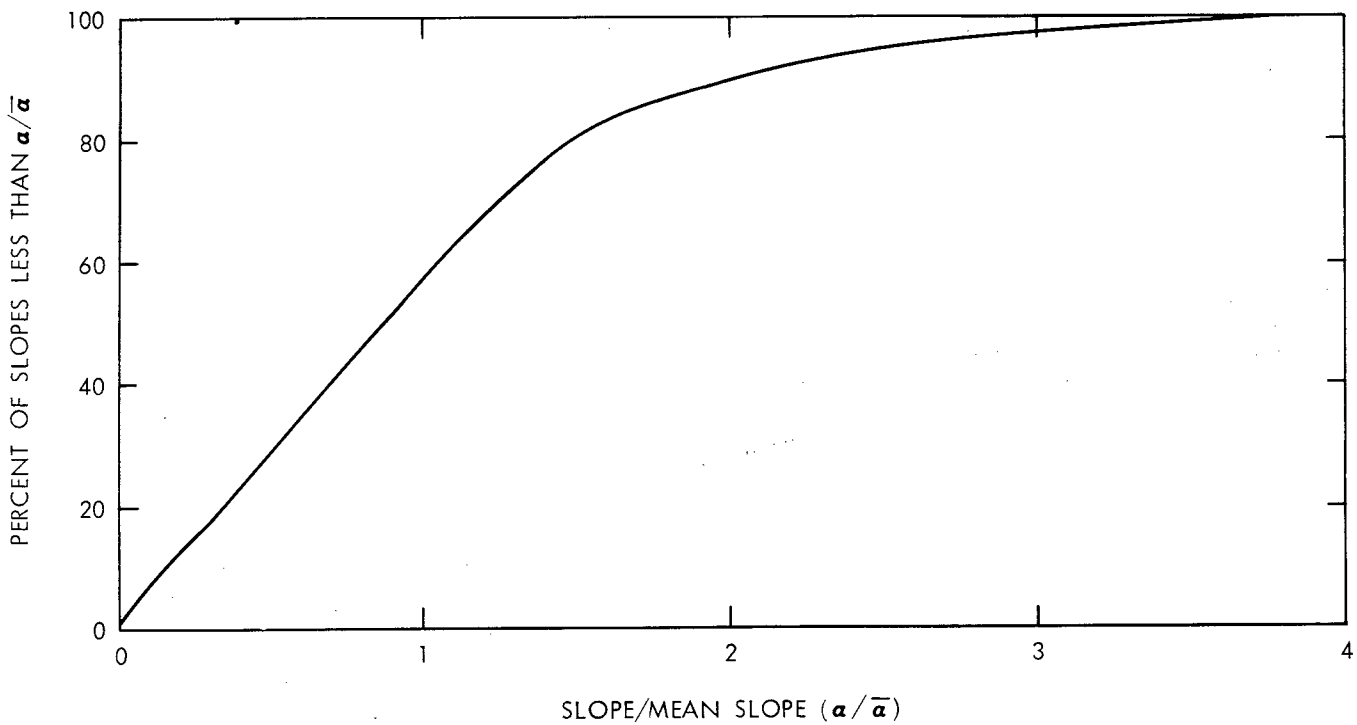

Figure 2. - Variation of cumulative terrain slope with nondimensional slope ratio (R. J. Pike).

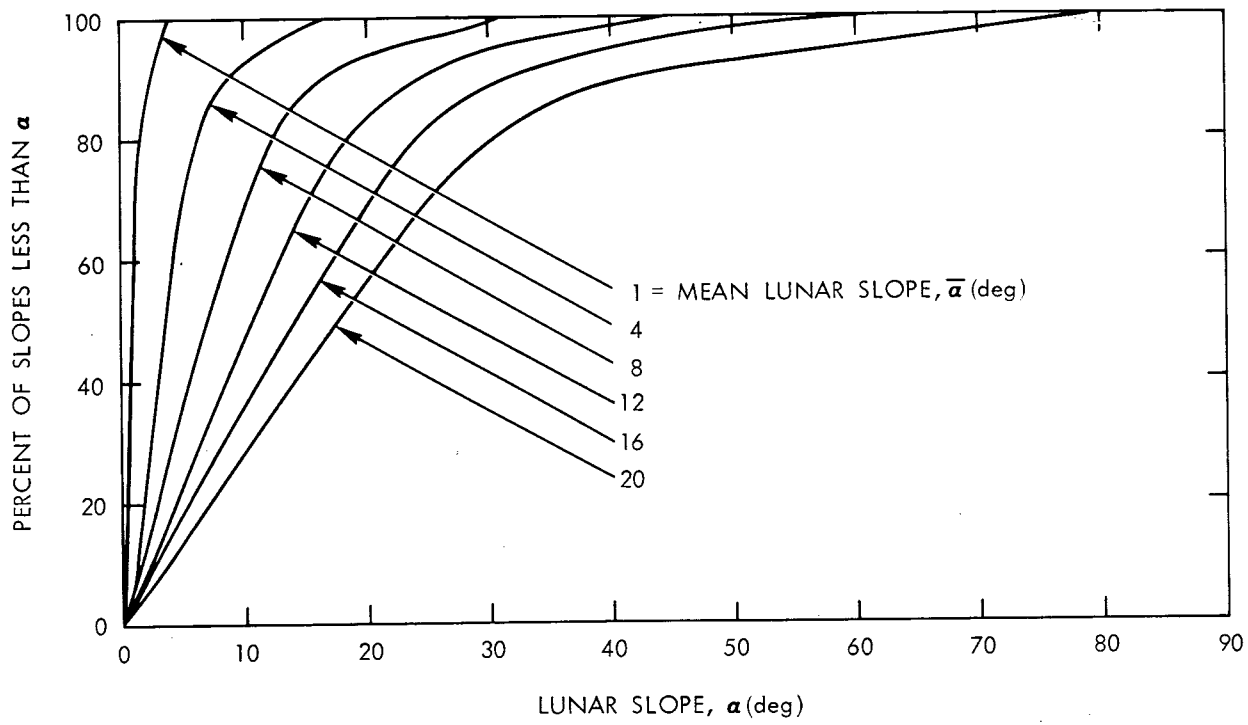

Figure 3. - Variation of cumulative terrain slope with mean lunar slope (R. J. Pike).

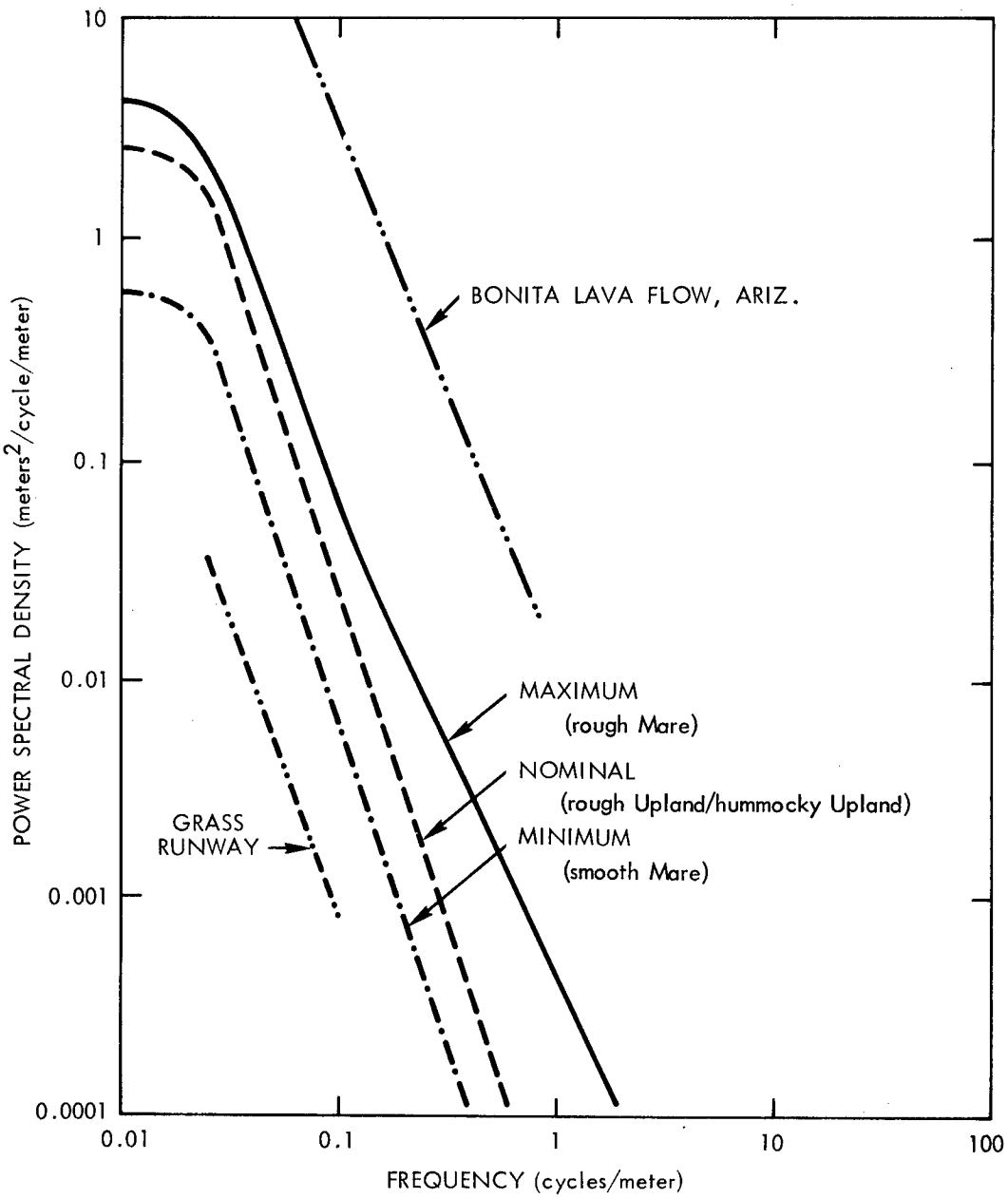

Figure 4. - Surface roughness - power spectral density vs. surface wave frequency (R. J. Pike).

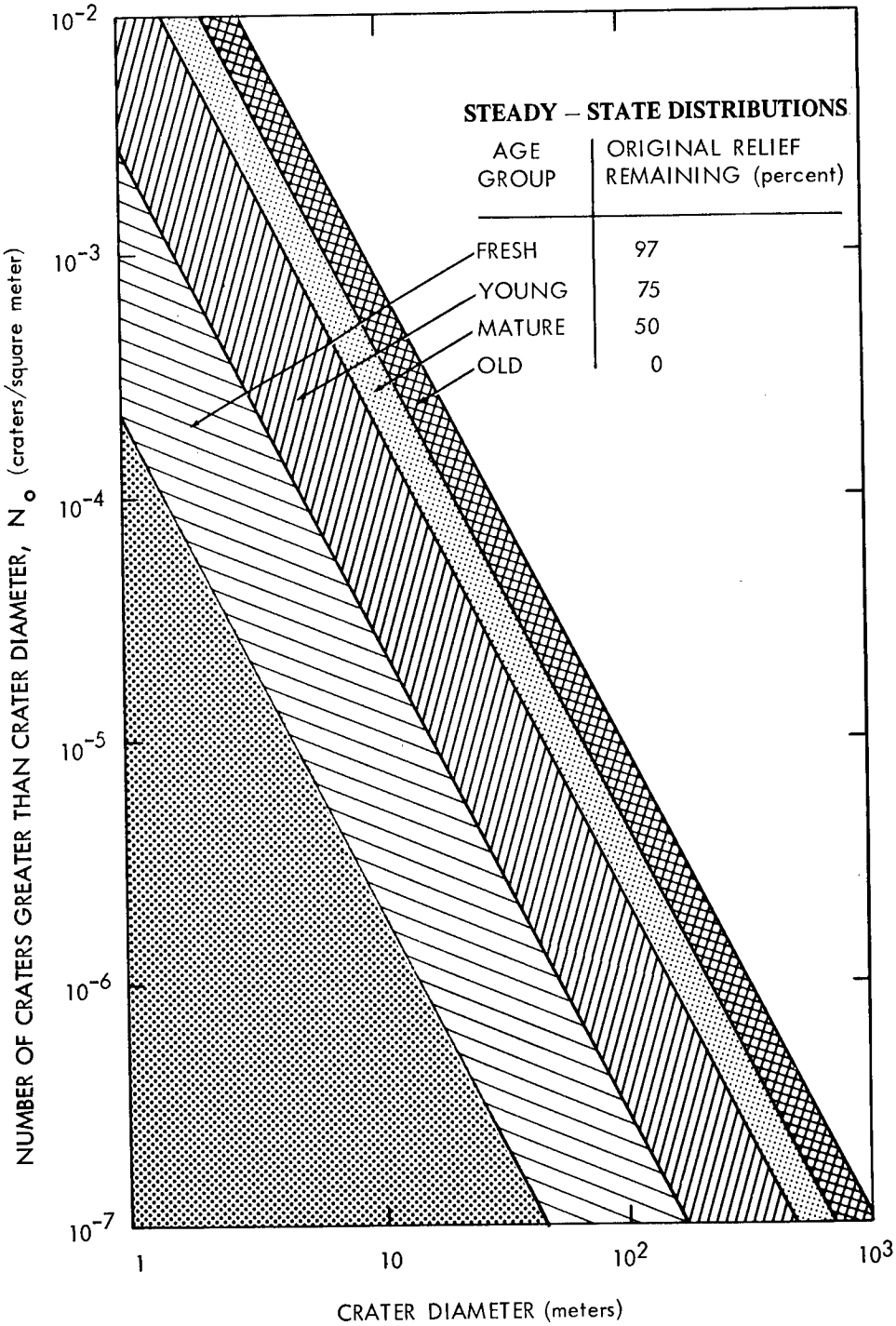

Figure 5. - Cumulative frequency and relief of craters for various age groups which occur on the smooth Mare, rough Mare, and Upland terrains (H. J. Moore)

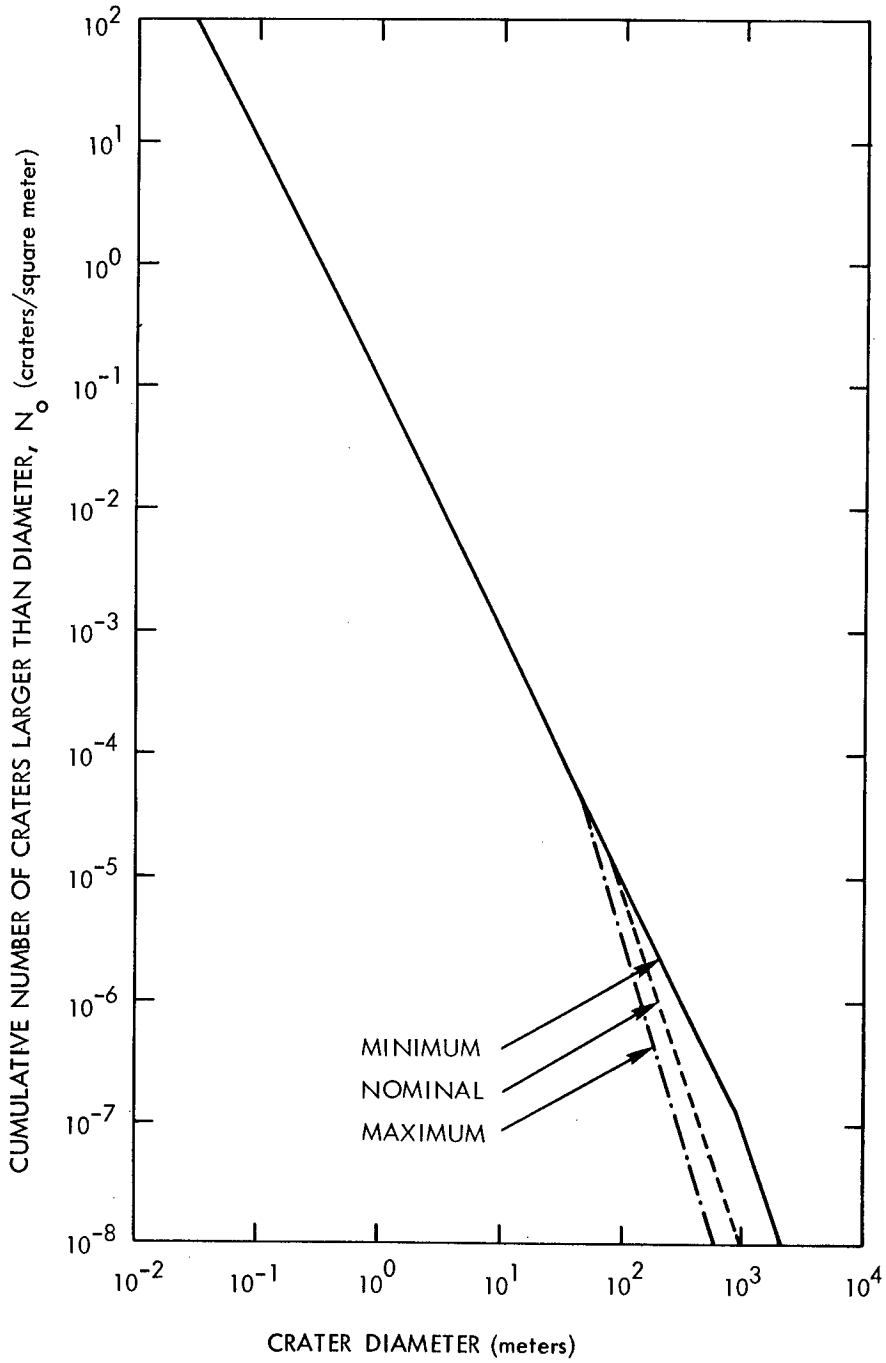

Figure 6. - Cumulative crater distribution for smooth Mare, rough Mare, and Upland terrains.

3.4 Lunar Blocks

For mobility studies the obstacle height should be considered equal to one-half the block diameter.

3.4.1 Block Properties

The dimension and shapes of blocks encompass a wide range. A standard lunar block is considered as one having a ratio of its longest dimension to its shortest dimension in the range of 1/1 to 1/5. Surfaces may be rounded or rectangular, may be pitted, eroded, or vesiculated. The standard height is considered to be equal to one-half the block diameter.

The blocks are gray in color, like the soil. Most are birghter than the fine soil material and have a normal albedo of 14 to 22 percent. Light reflected from some rocks showed polarization up to 30 percent at phase angles near 120°.

It is estimated that a typical lunar block has a density of 2.8 to 2.9 gm/cm^3 and a shearing strength of about 200 N/cm^2. (Data are based on one sample rock.)

3.4.2 Block Distributions in the Intercrater Region

Figure 7 shows the cumulative distribution of blocks in the intercrater regions, while figure 8 shows the percent of area covered by blocks of a given diameter per square meter.

3.4.3 Block Distributions Around Craters

Block distributions around craters vary from crater to crater (H. J. Moore). For interim design purposes the models shown in figures 9 and 10 are considered representative of blocky craters.

Figure 9 shows typical cumulative frequency distribution of blocks in the annular region between the crater rim and a distance two radii from the crater center (between R and 2R for a fresh crater). Figure 10 shows the corresponding percent of this area covered by blocks of a given diameter.

3.4.4 Block Fields

Studies (H. J. Moore) of dense block fields indicate the distributions may be higher than those shown in figure 9. However, Moore's data also show that there are often paths 50 meters or wider through even dense block fields which are relatively free of blocks.

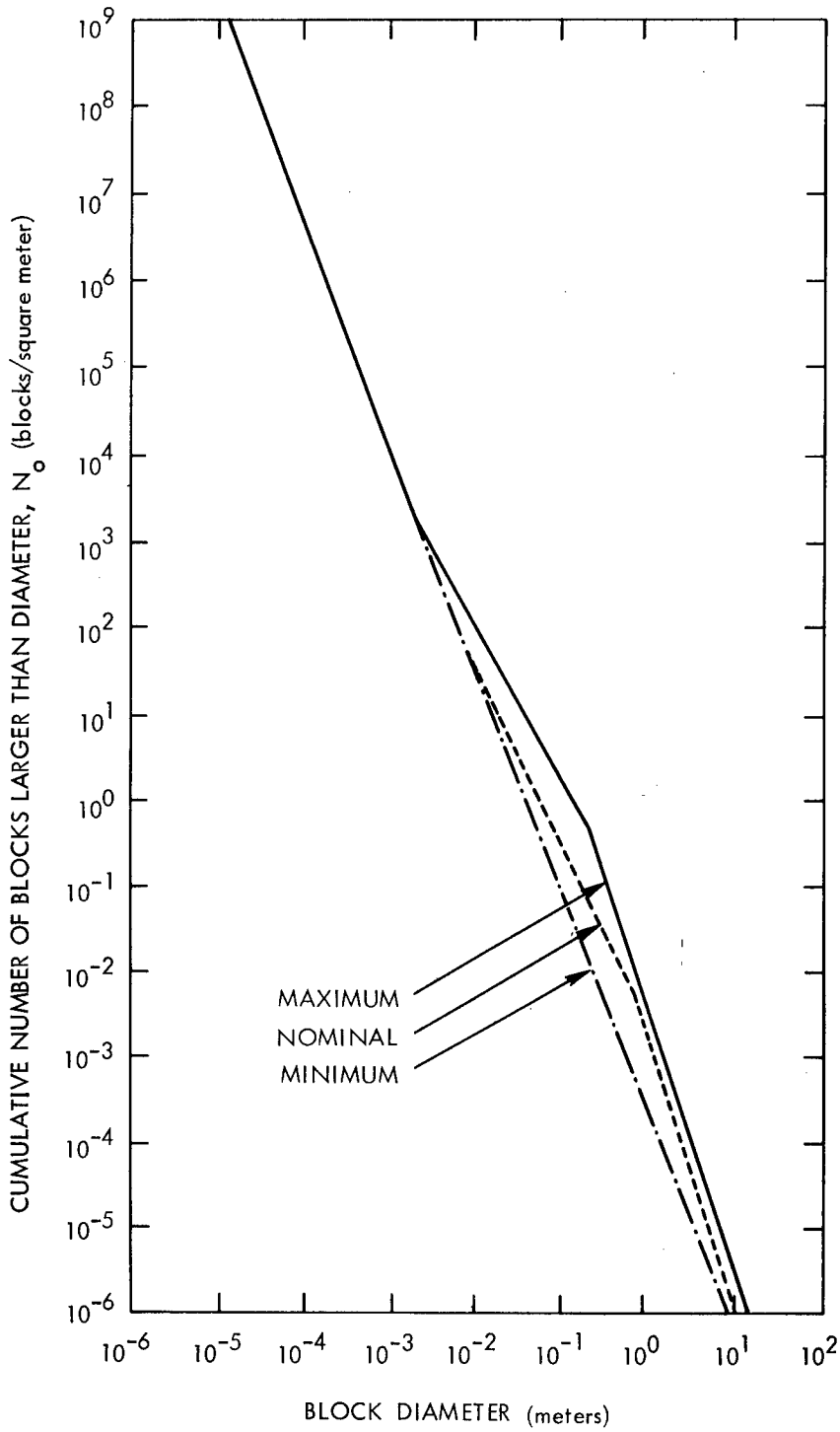

Figure 7. - Cumulative number of blocks in intercrater region of smooth Mare, rough Mare, and Upland terrains.

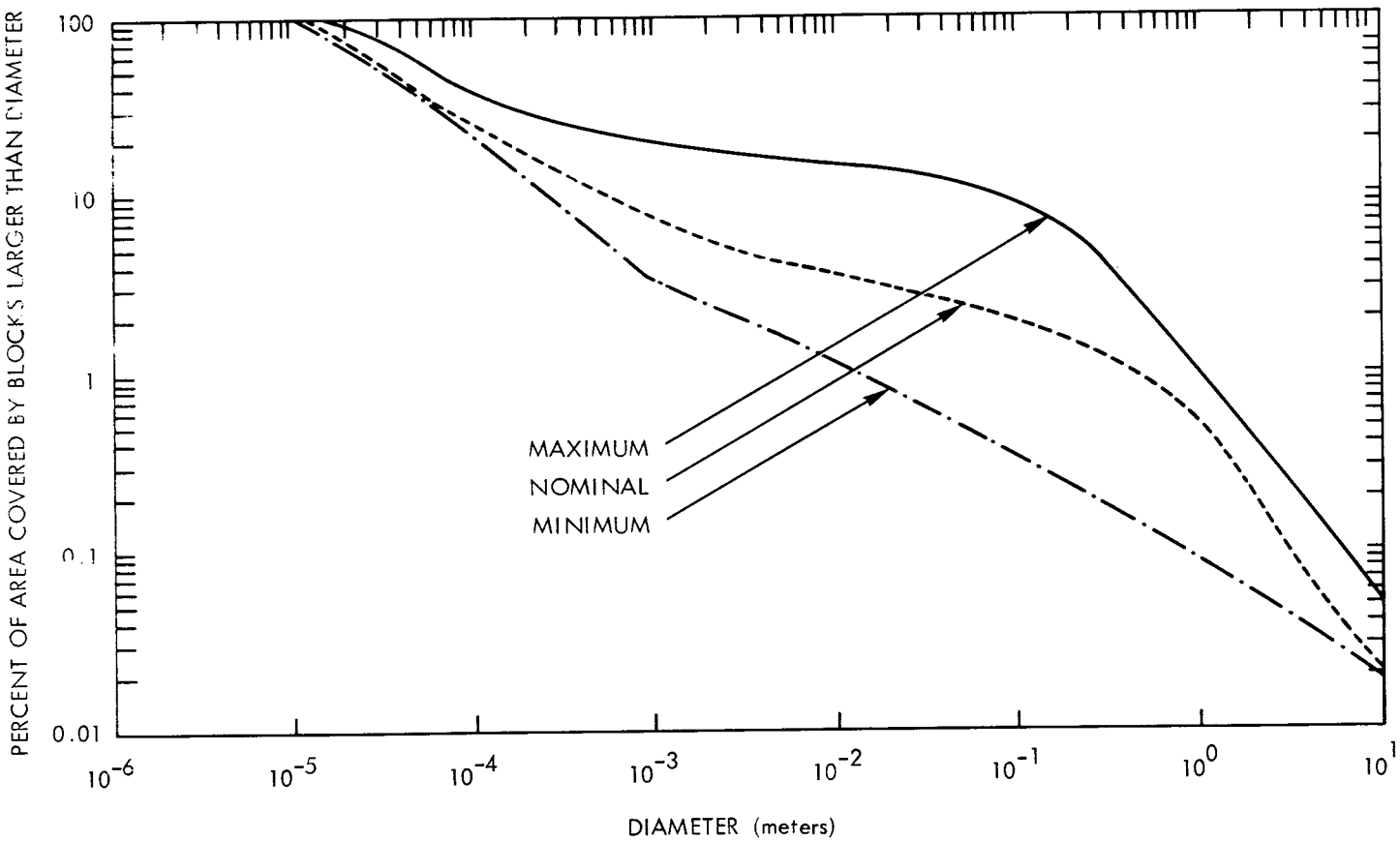

Figure 8. - Percent of intercrater area of smooth Mare, rough Mare, and Upland terrains which are covered by blocks.

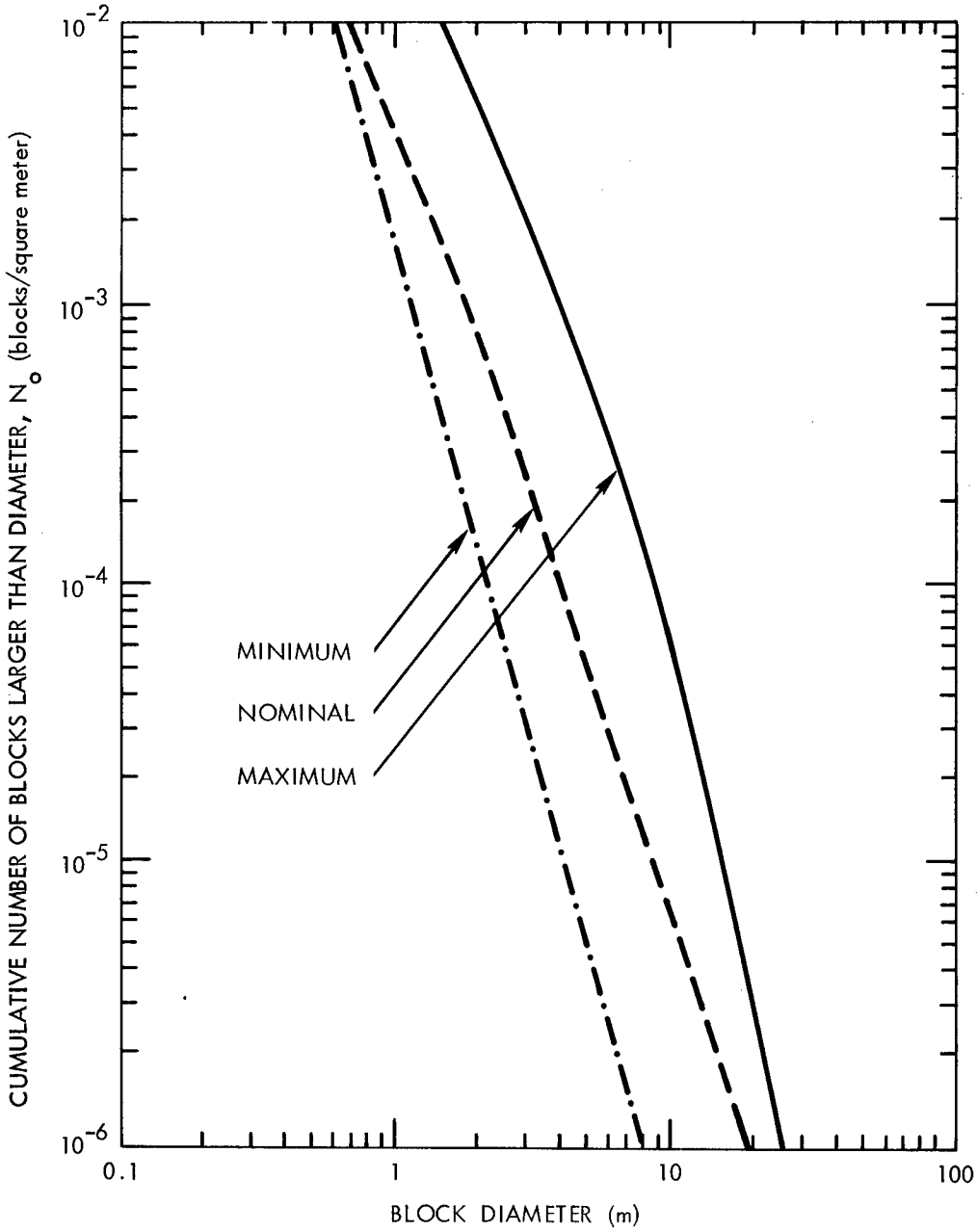

Figure 9. - Cumulative distribution of blocks between crater rim and two crater radii as seen around craters in smooth Mare, rough Mare, and Upland terrains.

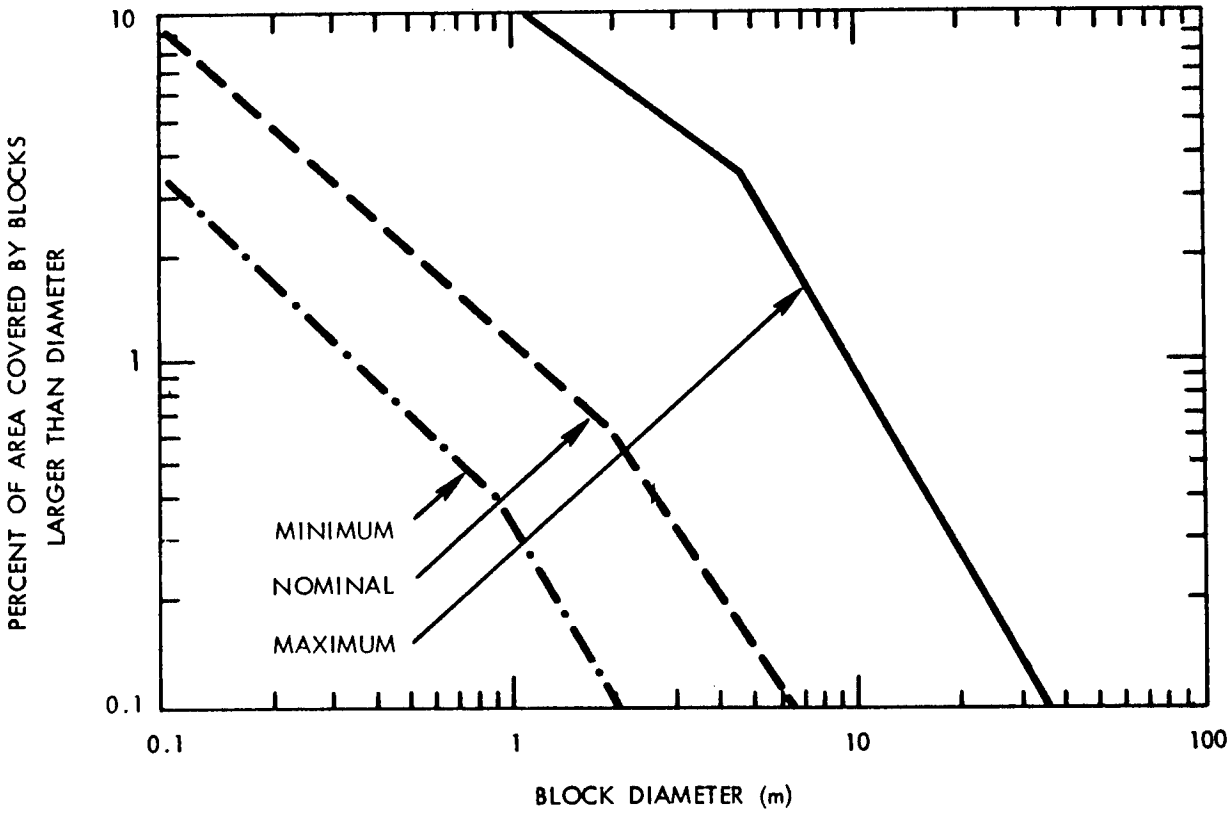

Figure 10. - Percent of area covered by blocks between crater rim and two crater radii as seen around craters in smooth Mare, rough Mare, and Upland terrains.

3.5 Soil Characteristics

The lunar surface soil material consists of a matrix of fine, partially cohesive particles, less than 1 mm in diameter with a few rocks scattered in and on the matrix. The most common elements of the soil layer are oxygen, silicon, and aluminum (as on Earth). The composition corresponds to that of a basaltic material and/or meteoritic basaltic achrondite material with some iron content.

3.5.1 Soil Parameters

Table V presents the average soil parameters; figure 11 shows the variation of static bearing capacity with penetration depth for soils on level ground. For soils on slopes, the bearing capacity can be determined by using reduction factors given in reference 68.

TABLE V

SOIL PARAMETERS

Parameter	Value
Composition (atomic percent) oxygen silicon aluminum	 60 20 7
Iron content (percent) Mare terrain Upland terrain	 5 2
Grain size (microns)	2 to 60
Cohesion (N/cm^2) nominal	0.02 to 0.2 0.05
Internal friction angle (deg)	31 to 39
Effective friction coefficient* (nondimensional) metal to soil or rock	 0.4 to 0.8
Adhesive strength (N/cm^2)	0.0025 to 0.01
Permeability (cm^2)**	$1x10^{-8}$ to $7x10^{-8}$
Seismic velocities (m/sec) compressional wave shear wave	 30 to 90 15 to 35
Bulk density (gm/cm^3) at 5 cm at 40 cm	 1.6 2.0
Porosity (nondimensional) at 5 cm depth	0.465

*Estimated from Surveyor landing dynamic simulations.

**Estimated from observed soil effects during Surveyor 5 vernier engine firing.

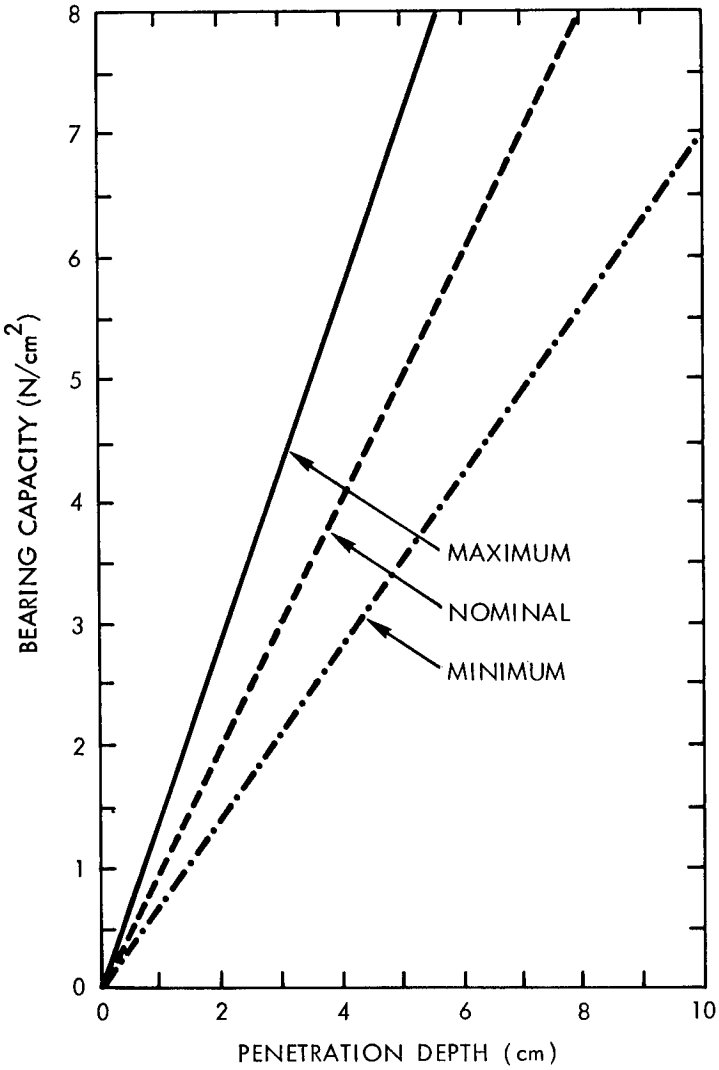

Figure 11. - Variation of static bearing capacity with depth.

3.6 Thermal Properties

3.6.1 Brightness Temperature

A Fourier series representation of measured equatorial brightness temperature (T_E) over a complete lunation period P is given by (ref. 33)

$$T_E = A_o + \sum_{n=1}^{50} A_n \cos \frac{2n\pi t}{P} + B_n \sin \frac{2n\pi t}{P} \tag{1}$$

The Fourier coefficients (A_n and B_n) are listed in table VI. Below a depth of about 1 meter the temperature remains constant at about 230° K (ref. 3).

A first order approximation for the variation of temperature with latitude (β) on the sunlit surface is given by

$$T = T_E \cos^{1/4} \beta \tag{2}$$

Lunar surface temperatures based on mathematical models for various values of the thermal inertia parameter (γ) are shown in figure 12. Saari and Shorthill (ref. 28) give isothermal and isophotic charts for 23 different phase angles.

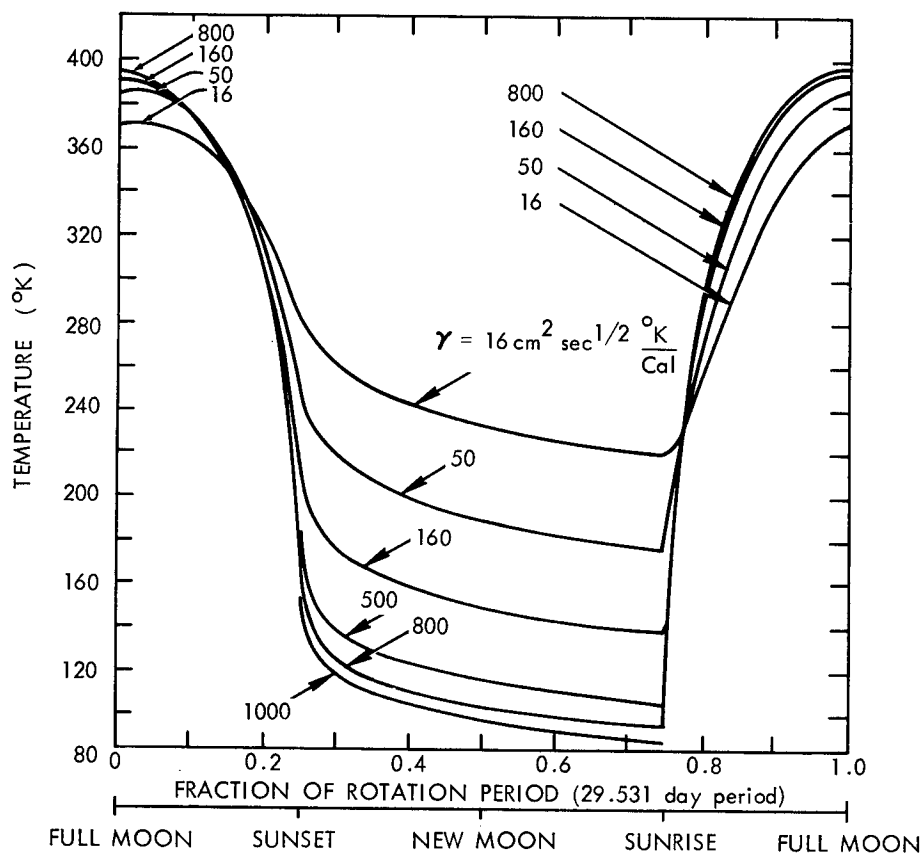

Figure 12. - Temperatures nearest surface for different thermal parameter values.

TABLE VI

FOURIER SERIES COEFFICIENTS

$A_o = 227.194$								
n	A_n	B_n	n	A_n	B_n	n	A_n	B_n
1	172.959	16.710	18	1.287	-0.2525	35	-0.6859	-1.395
2	30.978	-2.828	19	-2.292	-1.712	36	-0.6548	0.1242
3	-32.580	-5.861	20	-1.104	0.1936	37	0.5814	1.387
4	-11.958	1.437	21	1.990	1.620	38	0.6360	-0.1012
5	15.280	3.794	22	0.9928	-0.2003	39	-0.5067	-1.370
6	6.405	-0.8830	23	-1.707	-1.590	40	-0.6452	0.0698
7	-9.454	-2.819	24	-0.9227	0.1567	41	0.4118	1.351
8	-4.129	0.6055	25	1.486	1.522	42	0.6612	-0.0093
9	6.595	2.317	26	0.8615	-0.1585	43	-0.2845	-1.339
10	2.885	-0.5805	27	-1.235	-1.500	44	-0.6237	0.0645
11	-5.097	-2.161	28	-0.7767	0.1743	45	0.2027	1.369
12	-2.246	0.3976	29	1.063	1.499	46	0.5865	-0.01564
13	4.041	1.968	30	0.7044	-0.1354	47	-0.1762	-1.356
14	1.789	-0.3521	31	-0.9409	-1.457	48	-0.6448	-0.01454
15	-3.312	-1.921	32	-0.6887	0.1051	49	0.05244	1.329
16	-1.526	0.2377	33	0.8296	1.409	50	0.3160	0.000041
17	2.731	1.744	34	0.6733	-0.1237			

3.6.2 Brightness Temperature Directionality

An empirical expression, taking into account the directional aspects (ref. 32), has been developed for predicting the surface brightness temperature (T_B) of the sunlit portion in the infrared spectrum as follows

$$T_B = \left[\frac{\pi I_o}{\sigma}\right]^{1/4} \tag{3}$$

where

$$I_o\,(i, \varepsilon, g) = \frac{a_1 \cos i + a_2 \cos a'}{1 + a_4 \dfrac{\sin a'}{\cos i}} + \frac{a_3}{\pi}\left[(\pi - |g|)\cos |g| + \sin |g|\right] \tag{4}$$

and i, ϵ, ϕ_i, ϕ_ϵ, g are angles defined in figure 13, and

$$a = \frac{\pi}{2}\sqrt{\frac{i^2 + \epsilon^2 - 2i\epsilon \cos(\phi_i - \phi_\epsilon)}{\dfrac{\pi^2}{4} + \dfrac{4i^2\,\epsilon^2}{\pi^2} - 2i\epsilon \cos(\phi_i - \phi_\epsilon)}} \tag{5}$$

where

a_1 = 335 watts/m^2 - steradian
a_2 = 97.6 watts/m^2 - steradian
a_3 = 51.6 watts/m^2 - steradian
a_4 = 0.121

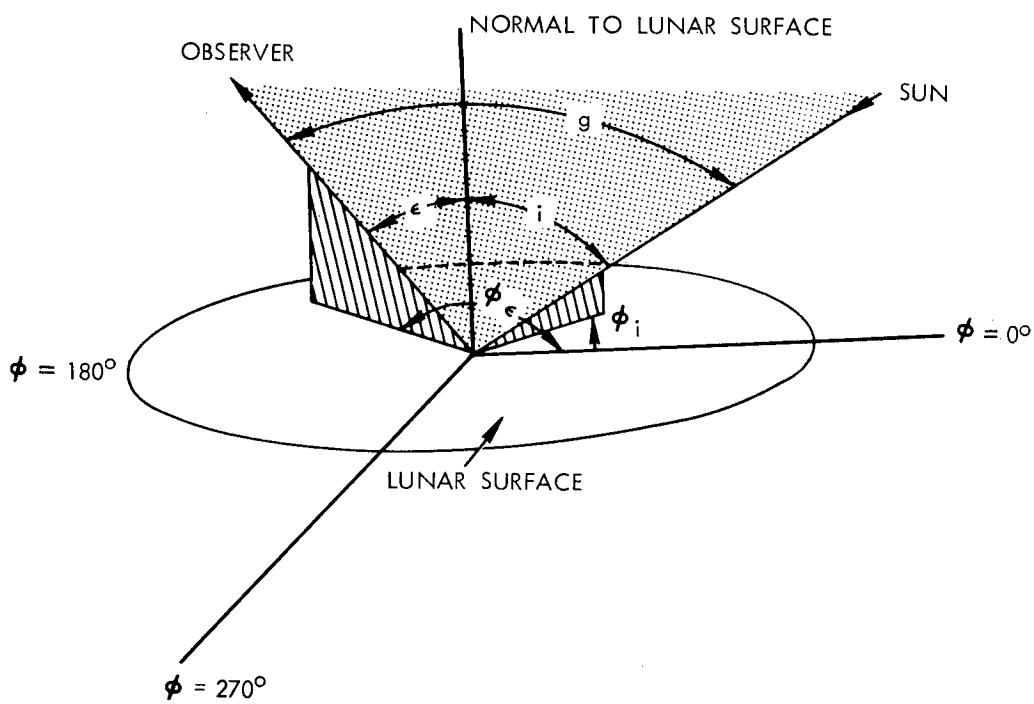

Figure 13. - Angles used in directionality analysis.

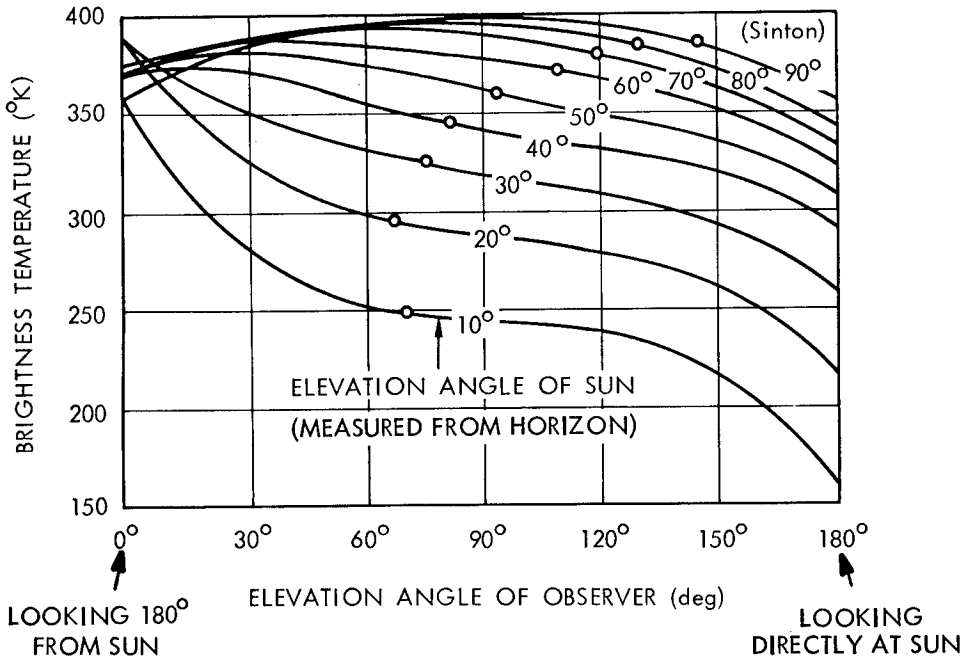

Figure 14. - Brightness temperature versus observer's elevation angle to the surface with the Sun at different elevation angles. The data for 90° Sun angle represents Sinton's (ref. 35) observations of the subsolar point. The Lambert temperature is indicated by the open circles (ref. 29). (Data (10°- 80°) fitted by least square polynomial approximations-Saari and Shorthill data)

The brightness directionality effect along the thermal meridian is shown graphically in figure 14 (ref. 29) as functions of Sun angle and elevation angle of observation. In terms of an observer on the surface as shown below, the 90° observer elevation angle corresponds to his looking vertically downward at the surface, 0° elevation angle to his looking at the horizon with the Sun on his back, and the 180° elevation angle to his looking at the horizon facing the Sun.

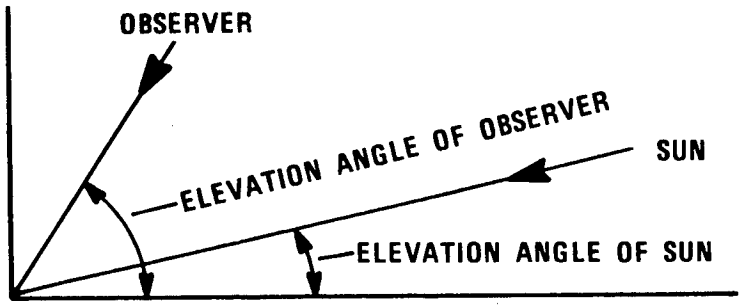

3.6.3 Surface Thermal Properties

Thermal conductivity, k, should be considered temperature-dependent and can be expressed as

$$k = k_o + k_1 T^3 \tag{6}$$

where T is the temperature, and k_o and k_1 are the conductive and reflectivity constants, respectively.

Laboratory data (ref. 55) for powdered pumice and basalt are used for the estimates of the conductivity constant, k_o, and reflectivity constant, k_1, given here.

$$2.5 < k_o \times 10^6 < 21 \text{ watt/cm}^\circ\text{K}$$

$$0.88 < k_1 \times 10^{13} < 3.57 \text{ watt/cm}^\circ\text{K}^4$$

These ranges should be considered as representative of the lunar soil.

The specific heat, c, is likely to be temperature-dependent, and the density, ρ, is depth-dependent. However, constant material thermal properties are useful as average properties for data comparison and environmental criteria.

Table VII lists recommended ranges for the thermal inertia parameter, γ, specific heat, c, conductivity, k, and density, ρ.

3.6.4 Thermal Radiation

The thermal radiation from the lunar surface is about 310 watts/m^2 at 1 AU with an average albedo of 0.110 (ref. 69).

3.7 Electrical Properties

3.7.1 Dielectric Constant and Loss Tangent

The complete range of values for the dielectric constant is about 1 to 8 where the high values are for solid material. The probable range is from 2 to 4 with the average value about 3. At a 2 to 3 cm wavelength, the value is about 2.4 ± 0.5 on the Mare and 3.3 ± 0.4 in the Upland (ref. 14). The relationship to wavelength can be approximated by the equation (ref. 22):

$$\epsilon = [1 + \rho\xi(\lambda)]^2 \,, \; \xi(\lambda) = 0.5 + 0.045 \ln\left(\frac{\lambda}{3}\right) \quad \text{for } 0.03 \text{ m} < \lambda < 200 \text{ m}. \tag{7}$$

The loss tangent, tan ϕ, lies in the range from 0.02 to 0.06, assuming a density of 1 to 2 gm/cm^3 (ref. 11).

TABLE VII

LUNAR SURFACE THERMAL PROPERTIES

Surface Material	Parameter, γ $cm^1\ sec^{1/2}\ °K/joule$ ($cm^2\ sec^{1/2}\ °K/cal$)	Density, ρ kg/m^3 (gm/cm^3)	Specific Heat, c joule/kg °K (cal/gm °K)	Conductivity, k watt/m °K (cal/cm sec °K)
Total range	5.97–334 (25–1400)	500–3000 (0.5–3)	755–1007 (0.18–0.24)	2.14×10^{-3} - 1.13 (5.1×10^{-6} - 2.7×10^{-3})
Range for particulate material heavily mixed with blocks	57.2–119 (240–500)	1200–2000 (1.2–2.0)	837 (0.20)	7.12×10^{-3} - 1.8×10^{-2} (1.7×10^{-5} - 4.3×10^{-5})
Blocks (rocks)	7.2 (30)	2500 (2.5)	837 (0.20)	9.22×10^{-1} 2.2×10^{-3}
Range, excluding blocks	95.5–238 (400–1000)	500–1100 (0.5–1.1)	837 (0.20)	4.18×10^{-3} - 1.17×10^{-2} (1×10^{-5} - 2.8×10^{-5})
Average maria	95.5–191 (400–800)	800–1500 (0.8–1.5)	837 (0.20)	4.18×10^{-3} - 8.8×10^{-2} (1×10^{-5} - 2.1×10^{-5})

3.8 Optical Properties

3.8.1 Normal Albedo

Normal albedo values for the front and rear faces of the Moon are listed in table VIII. Table IX gives normal albedo values for some prominent features on the front face.

3.8.2 Photometric Model

The luminance, B, of the lunar surface is related to the photometric function, ϕ, the solar constant, E (1400 watts/m^2 at 1 AU), and the normal albedo, ρ_o, by the equation

$$B = \frac{E}{\pi} \rho_o \phi \tag{8}$$

where the function, ϕ, depends on the phase angle, g, and surface orientation angle, a, as shown in figure 15.

Figure 15 (a) shows the location of a section of the lunar surface being observed along with the direction of the Sun line and observation direction. The Sun line and observation direction define a plane, called the phase plane, which is independent of the orientation of the lunar surface plane being observed. The phase angle is the angle in the phase plane (also independent of orientation of observed lunar surface area) between the Sun line and line of observation. The angle a, is an angle in the phase plane between the viewing direction and a line perpendicular to the line of intersection of the phase plane and lunar surface plane. The angle, a, is positive when the viewing line lies between the solar vector and the perpendicular line. Illustrations of positive and negative a are shown in figure 15 (b).

Figures 16 and 17 display the variation of the photometric function with angles g and a (ref. 47).

3.8.3 Polarization of Moonlight

Electromagnetic vibrations in the light emanating from the Sun are distributed fairly equally in planes in all directions. After reflection from the Moon the intensities in different planes no longer are equal. The portion of polarized light is defined by

$$P_I = \frac{I_1 - I_2}{I_1 + I_2} \tag{9}$$

TABLE VIII

NORMAL ALBEDO VALUES OF FRONT AND BACK FACES OF THE MOON

Regions	Normal Albedo		
	Minimum	Maximum	Average (peak value)
Front Side			
Mare	0.07	0.12	0.095
Upland	0.108	0.24	0.150
Entire face	0.07	0.24	0.110
Back Side			
Entire face			0.217

where I_2 is the intensity of the reflected light in the plane defined by the incident and reflected light paths (phase plane) and I_1 is the intensity in the plane at right angles. The polarization curves for the Moon shown in figure 18 for both the waxing and waning Moon were obtained by Lyot (ref. 70, also presented in ch. 9 of ref. 38). The differences in polarization are attributed to the distributions of the Maria which have unusually large polarization and occupy about twice as much area at last quarter as at first quarter. The polarization changes in roughly inverse proportion to the albedo.

3.9 Lunar Atmosphere

The lunar atmosphere is nearly nonexistent and will have a negligible effect on spacecraft except for problems associated with the effects of vacuum on components and materials. Estimates of atmospheric pressure and density are given in table II.

TABLE IX

NORMAL ALBEDO FOR SELECTED LUNAR FEATURES

Lunar Feature	Reference 40	Reference 42	Reference 44
Darkest Point	0.05	0.0516	0.070
Brightest Point	0.18	0.2190	0.240
Mare Crisium	0.062	0.0631–0.0784	0.085–0.096
Mare Fecunditatis	0.069	0.0655	0.090–0.108
Oceanus Procellarum	0.051–0.070	0.0533–0.0737	0.079–0.096
Sinus Iridum	0.065	0.0674	0.085–0.096
Mare Tranquillitatis	0.066	0.0571–0.0668	0.085–0.108
Mare Serenitatis	0.070	0.0585–0.0692	0.090–0.114
Mare Frigoris	0.089	0.0738	0.102–0.127
Mare Imbrium	0.054–0.074	0.0632	0.086–0.102
Mare Vaporum	0.060	0.0657	0.090–0.108
Mare Nubium	0.062–0.073	0.0627–0.0705	0.090–0.108
Tycho	0.154	0.0742–0.1737	0.150–0.169

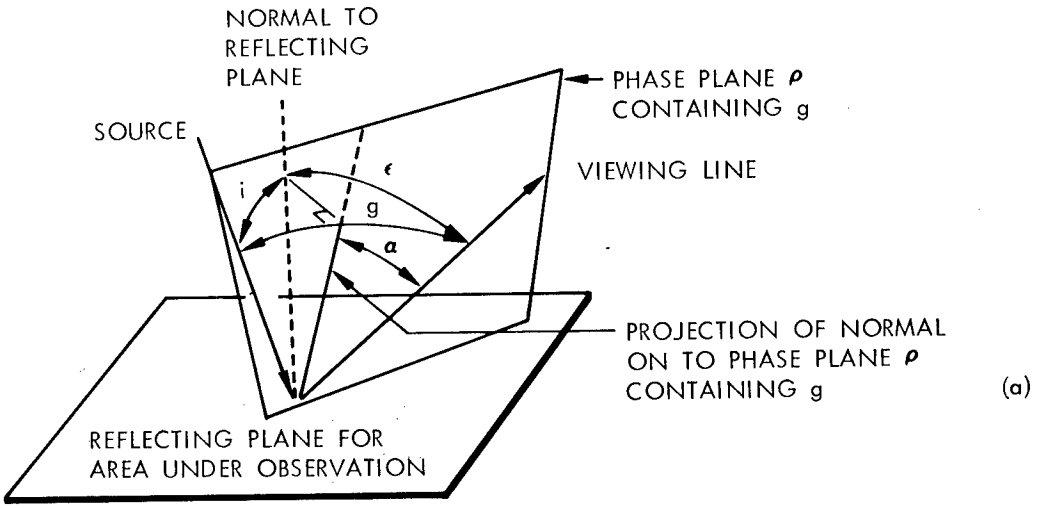

i ANGLE OF INCIDENCE
ε ANGLE OF EMITTANCE
g PHASE ANGLE
α PROJECTION OF ANGLE ε ONTO PHASE PLANE ρ

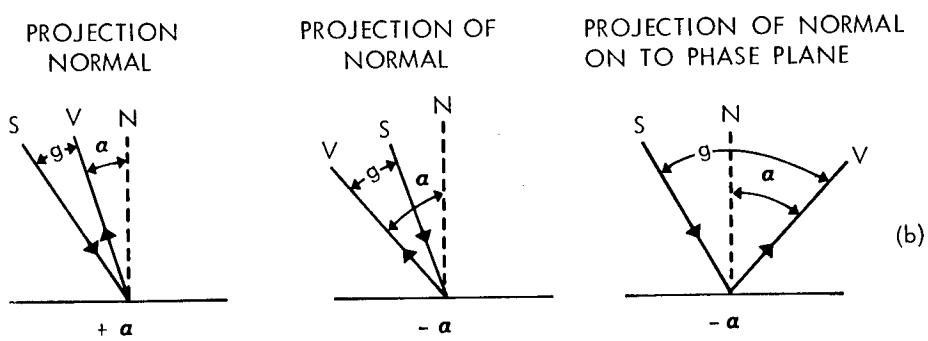

Figure 15. - Photometric Model Geometry,
(a) geometry, (b) positive and negative α.

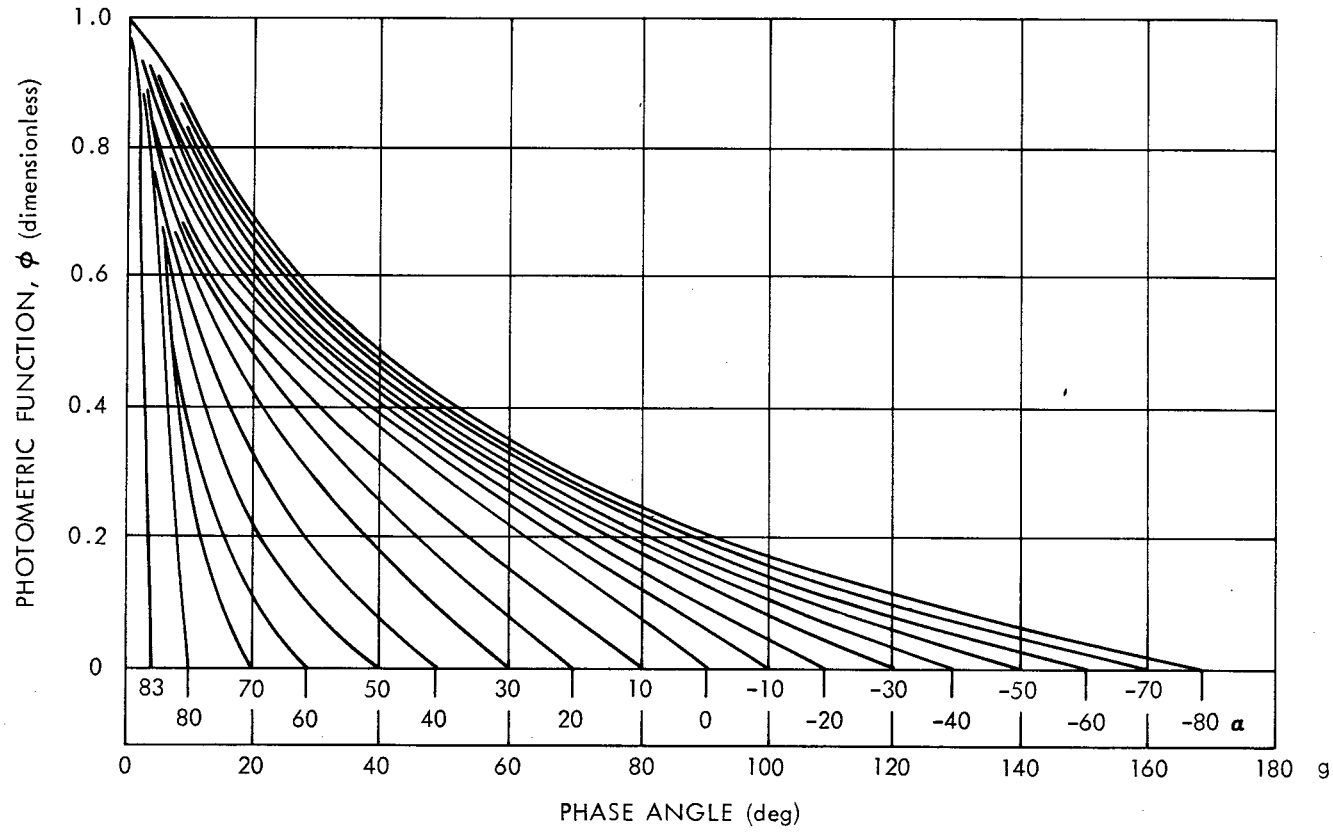

Figure 16. - Variation of photometric function with phase angle g and angle α (after Fedoretz, ref. 47).

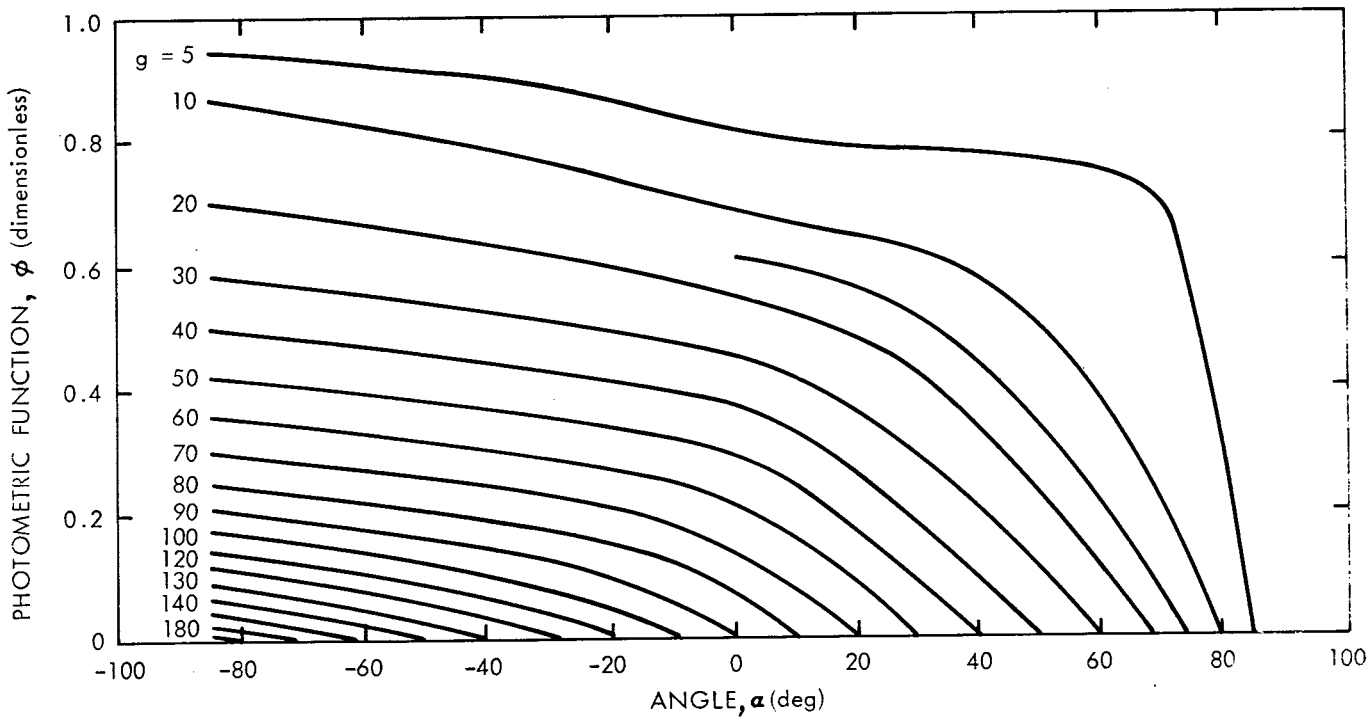

Figure 17. - Variation of photometric function with angle α and phase angle g (after Fedoretz, ref. 47).

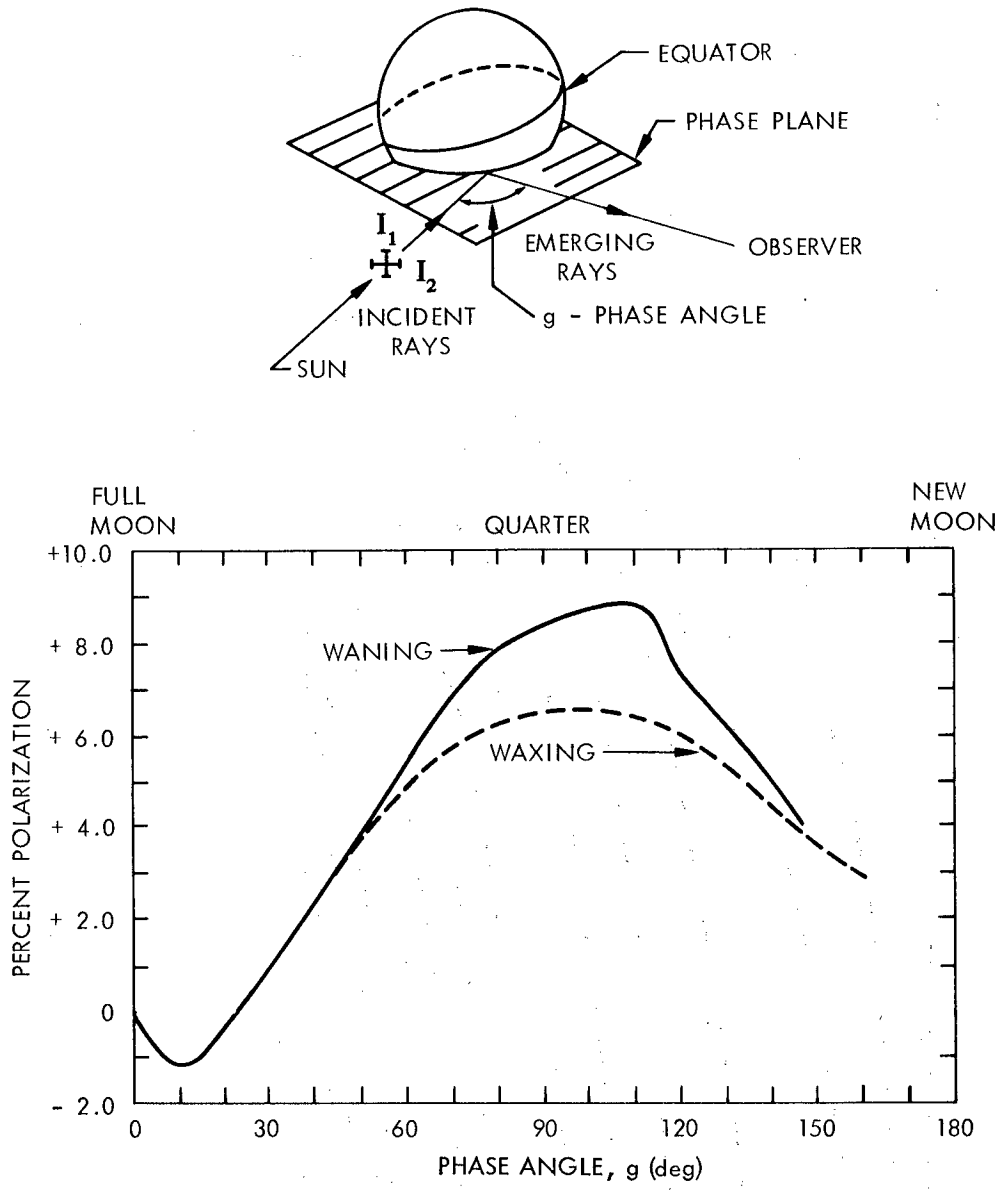

Figure 18. - Polarization of lunar surface as a function of phase angle g (after Lyot, ref. 70).

REFERENCES

1. Vaughan, O. H.: Lunar Environment: Design Criteria Models for Use in Lunar Surface Mobility Studies. NASA TM X–53661, Sept. 28, 1967.

2. Smith, R. E.: Space Environment Criteria Guidelines for Use in Space Vehicle Development (1968 Revision). NASA TM X–53798, Oct. 31, 1968.

3. Glasstone, S.: Sourcebook on the Space Sciences. D. Van Nostrand Company, Inc., Princeton, New Jersey, 1965.

4. Rowan, L. C.; and McCauley, J. R.: Lunar Terrain Analysis. Lunar Orbiter-Image Analysis Studies Report, U.S. Geological Survey Report, May 1, 1965 to Jan. 31, 1966, pp. 89–129.

5. McCauley, J. F.: Terrain Analysis of the Lunar Equatorial Belt. U.S. Geological Survey open-file report, July 1, 1964.

6. Anon.: Photometric Techniques For Mapping Orbiter Site II S-2. Aeronautical Chart and Information Center, NASA Defense Purchase Request No. T–55866, Feb. 1968.

7. Rozema, W.: The Use of Spectral Analysis in Describing Lunar Surface Roughness. Interagency Report: Astrogeology 12, U.S. Geological Survey, Dec. 1968.

8. Jaeger, R. M.; and Schuring, D. J.: Spectrum Analysis of Terrain of Mare Cognitum. J. Geophys. Res., vol. 71, no. 8, April 1966, pp. 2023–2028.

9. Anon.: Surveyor VII Mission Report, Part II: Scientific Results. Jet Propulsion Lab., Tech. Rept. 32–1264, March 15, 1968.

10. Anon.: Surveyor I Mission Report, Part II: Scientific Results. Jet Propulsion Lab., Tech. Rept. 32–1023, Sept. 10, 1966.

11. Anon: Surveyor III Mission Report, Part II: Scientific Results. Jet Propulsion Lab., Tech. Rept. 32–177, June 1, 1967.

12. Anon: Surveyor V Mission Report, Part II: Scientific Results. Jet Propulsion Lab., Tech. Rept. 32–1246, Nov. 1, 1967.

13. Anon: Surveyor VI Mission Report, Part II: Scientific Results. Jet Propulsion Lab., Tech. Rept. 32–1262, Jan. 10, 1968.

14. Anon: Surveyor Project Report. Jet Propulsion Lab., Tech. Rept. 32–1265.

15. Vinogradov, A. P.; Surkov, Yu. A.; Cherkasov, I. I.; and Shvarev, V. V.: Lunar Surface Explorations with SovietAutomatic Stations "Luna-9" to "Luna-13". Presented by the Government of the USSR to the U.N. Conf. on the Exploration and Peaceful Uses of Outer Space, May 1968.

16. Cherkasov, I. I.; Vakhnin, V. M.; Kemurjian, A. L.; Mikhalov, L. N.; Mikheyev, V. V.; Musatov, A. A.; Smorodinov, M. I.; Shvarev, V. V.: Determination of the Density and Mechanical Strength of the Surface Layer of the Lunar Crust at the Landing Site of Luna 13 Automatic Lunar Landing Station. Paper presented at the 10th plenary meeting of Cospar, London, July 1967; published in Kosmicheskie Issledovaniia, 5, 1967 pp. 746-757.

17. Cherkasov, I. I.; and Shvarev, V. V.: First Results of the Intimate Investigations of the Lunar Soil. Academia Nauk SSSR, 1968.

18. Jaffe, L. D.: Results of the Surveyor Lunar Landings. Presented at the Symposium of Physics of the Moon and Planets, Academy of Sciences of the USSR, Kiev, Ukraine, October 15, 1968.

19. Terzaghi, I.; and Peck, R. B.: Soil Mechanics in Engineering Practice. John Wiley and Sons, New York, 1964.

20. Scott, R. F.: The Density of the Lunar Surface Soil. J. Geophys. Res., vol. 73, no. 16, August 15, 1968.

21. Matveev, Y. G.; Suchkin, G. L.; and Troitskii, V. S.: Change of Lunite Density with Depth in the Surface Layer. Soviet Astronomy, vol. 9, No. 4, Jan.-Feb. 1966, pp. 626-631. (Translated from Astronomicheskii Zhurnal, vol. 42, no. 4, July-Aug. 1965, pp. 810-816.)

22. Tikhonova, T. V.; and Troitskii, V. S.: The Spectrum of the Reflection Coefficient with Changing Lunar Material Properties Into the Depth. Presented at the Symposium of Physics of the Moon and Planets, Academy of Sciences of the USSR, Kiev, Ukraine, October 15, 1968.

23. Jones, B. P.: Density-Depth Model for the Lunar Outermost Layer. J. Geophys. Res., vol. 73, no. 24, Dec. 15, 1968, pp. 7631-7635.

24. Gault, D. E.; Quaide, W. L.; and Oberbeck, V. R.: Interpreting Ranger Photographs from Impact Cratering Studies. Chapter 6, The Nature of the Lunar Surface, W. N. Hess, ed., The Johns Hopkins Press, Baltimore, Maryland, 1966.

25. Oberbeck, V. R.; and Quaide, W. L.: Estimated Thickness of a Fragmental Surface Layer of Oceanus Procellarum. J. Geophys. Res., vol. 72, no. 18, Sept. 15, 1967.

26. Quaide, W. L.; and Oberbeck, V. R.: Thickness Determinations of the Lunar Surface Layer from Lunar Impact Craters. J. Geophys. Res., vol. 73, no. 16, August 15, 1968.

27. Paterson, N. R.: Seismic Wave Propagation in Porous Granular Media. Geophysics, vol. XXI, no. 3, July 1956, pp. 691-714.

28. Saari, J. M.; and Shorthill, R. W.: Isothermal and Isophotic Atlas of the Moon (Contours through a Lunation). NASA CR-855, Sept. 1967.

29. Saari, J. M.; and Shorthill, R. W.: Review of Lunar Infrared Observations. Physics of the Moon, S. F. Singer, ed., vol. 13, AAS Science and Technology Series, 1967, pp. 57-99.

30. Murray, B. C.; and Wildey, R. L.: Surface Temperature Variations During the Lunar Nighttime. Astrophysical J., vol. 139, pp. 734-750, 1964.

31. Montgomery, C. G.; Saari, J. M.; Shorthill, R. W.; and Siz, Jr., N. F.: Directional Characteristics of Lunar Thermal Emission. Brown Engineering Res. Labs. Technical Note R-213, and Boeing Document DI-82-0568, 1966.

32. Ashby, N.; and Burkhard, D. G.: A Study of Radiative Aspects of Lunar Materials. NASA CR-61481, Jan. 1967.

33. Calvert, T. A.: Thermal and Dielectric Properties of a Homogeneous Moon Based on Microwave and Infrared Temperature Observations. NASA TM X–1734, Feb. 1969.

34. Low, F. J.: Lunar Nighttime Temperatures Measured at 20 Microns. Astrophysical J., vol. 142, 1965, pp. 806-808.

35. Sinton, W. M.: Temperatures on the Lunar Surface. (Physics and Astronomy of the Moon, Z. Kopal, ed., Academic Press, 1962) pp. 407-427.

36. Wildey, R. L.; Murray, B. C.; and Westphal, J. A.: Reconnaissance of Infrared Emission from the Lunar Nighttime Surface. J. Geophys. Res., vol 72, no. 14, July 15, 1967, pp. 3743-3749.

37. Winter, D. F.; and Saari, J. M.: A New Thermophysical Model of the Lunar Soil. Document DI-82-0725, Boeing Scientific Research Laboratories, 1968.

38. Kuiper, G. P.; and Middlehurst, B. M., eds.: Planets and Satellites. The Solar System III, Photometry of the Moon, Chap. 6 by Minnaert, M.; Univ. of Chicago Press, 1961.

39. Ziedman, K.: Lunar Surface Visibility. Report prepared by TRW Systems for the Manned Spacecraft Center under Contract NAS 94810, Report No. 05952-6011-R000, Aug. 3, 1966.

40. Sytinskaya, N. N.; and Sharonov, V. V.: Study of the Reflecting Power of the Moon's Surface. Trudy Leningrad Obs., vol. 16, 1952 (Translated by STL, Inc., STL-TR-61-5110-23, May 1961).

41. Van Digglen, J.: Photometric Properties of Lunar Crater Floors. Res. Astr. Obs., Utrecht, Netherlands, vol. 14, no. 2, 1959. Translated, NASA-TT-F-209, Aug. 1964.

42. Shorthill, R. W.; Saari, J. M.; Baird, F. E.; and LeCompte, J. R.: Photometric Properties of Selected Lunar Features. Report prepared by The Boeing Company for the NASA Manned Spacecraft Center under Contract NAS 9-7665, Sept. 1968.

43. Gehrels, T.; Coffeen, T.; and Orvings, D.: Wavelength Dependence of Polarization. III. The Lunar Surface. The Astron. J., vol. 69, no. 10, Dec. 1964, pp. 826-852.

44. Pohn, H. A.; and Wildey, R. L.: A Photoelectric-Photographic Map of the Normal Albedo of the Moon. Astrogeologic Studies Annual Progress Report, July 1, 1965 to July 1, 1966, U. S. Geological Survey, pp. 211-234.

45. Hapke, B.: A Theoretical Photometric Function for the Lunar Surface. J. Geophys. Res., vol. 68, pp. 4571-4586, 1963.

46. Hapke, B.: An Improved Theoretical Lunar Photometric Function. Astron. J., vol. 7, no. 5, 1966, pp. 333-339.

47. Fedoretz, V. A.: Photographic Photometry of the Lunar Surface. Reports of the Astron. Observatory of the Charkow State University, vol. 2., 1952.

48. Herriman, A.; Washburn, H.; and Willingham, D.: Ranger Preflight Science Analysis and the Lunar Photometric Model. Jet Propulsion Lab., Tech. Rept. 32-384, 1963.

49. Willingham, D.: The Lunar Reflectivity Model for Ranger Block III Analysis. Jet Propulsion Lab.,Tech. Rept. 32-664, 1964.

50. Watson, K.: Photoclinometry From Spacecraft Images. U. S. Geological Survey Professional Paper 559–B, 1968.

51. Thompson, T. W.: A Study of Radar-Scattering Behavior of Lunar Craters at 70 cm. Research Report RS 64, Cornell University Center for Radio-physics and Space Research, Ithaca, New York, 1965.

52. Tyler, G. L.: Oblique-Scattering Radar Reflectivity of the Lunar Surface: Preliminary Results from Explorer 35. J. Geophys. Res., vol. 73, no. 24, Dec 15, 1968, pp. 7609-7630.

53. Tyler, G. L.: Brewster Angle of the Lunar Crust. Nature, vol. 219, no. 5160, pp. 1243-1244, Sept. 21, 1968.

54. Yakovlev, O. E.; and Yefimov, A. E.: An Investigation of the Reflection of Meter Radio-Waves from the Surface of the Moon. Doklady, Akademiia, Nauk, SSSR, vol. 174, pp. 583-584, 1967 (in Russian).

55. Wechsler, A. E.; and Simon, I.: Thermal Conductivity and Dielectric Constant of Silicate Materials. Arthur D. Little, Inc., Contract Report NAS8-20076, December 1966.

56. Fensler, W. E.; Knott, E. F.; Olte, A.; and Siegel, K. M.: The Electromagnetic Parameters of Selected Terrestrial and Extra-terrestrial Rocks and Glasses. The Moon, A. Kopal; and Z. K. Mikhailov, eds., Academic Press, 1962, pp. 545-565.

57. Gringauz, K. I.; Bezrukikh, V. V.; Khakhlov, M. Z.; Zastenker, G. N.; Remizov, A. P.; and Musatov, L. S.: The Results of Experiments for Determining the Lunar Ionosphere Conducted by the First Artificial Luna Satellite. Doklady, Akademija, Nauk SSSR, vol. 170, no. 6, 1966 (in Russian).

58. York, W.; and Savely, R. T.: Directory of Standard Geodetic and Geophysical Constants for Gemini and Apollo. NASA General Working Paper No. 10, 020B, Manned Spacecraft Center, April 6, 1966.

59. Urey, H. C.: The Contending Moons. Astronautics and Aeronautics, Jan. 1969, pp. 37-41.

60. Muller, P. M.; and Sjogren, W. L.: Consistency of Lunar Orbiter Residuals with Trajectory and Local Gravity Effects. Jet Propulsion Lab. Tech. Rept. 32-1307, Sept. 1, 1968.

61. Tolson, R. H.; and Gapcynski, J. P.: An Analysis of the Lunar Gravitational Field as Obtained from Lunar Orbiter Tracking Data. NASA Langley Research Center, Paper presented at the IQSY/COSPAR Assemblies, London, July 17-28, 1967.

62. Anon.: Survey and Program Definition for Off-Road Mobility Research. Cornell Aeronautical Laboratories TR CAL VJ-2330-G-1, March 7, 1967.

63. Bekker, M. G.: Theory of Land Locomotion, The University of Michigan Press, Ann Arbor, Michigan, 1962.

64. Bekker, M. G.: Mechanics of Off-The-Road Locomotion. James Clayton Lecture presented at an Ordinary Meeting of the Institution of Mechanical Engineers, London, Nov. 13, 1962.

65. Peters, J. D.: Trafficability of the Lunar Surface Considering the Bearing Capacity and Failure Modes of Lunar Surface Materials. Space Age Facilities, ASCE Aero-Space Transport Div. Speciality Conference, Cocoa Beach, Florida, Nov. 17-19, 1965. Proceedings A67-16606 05-11, New York ASCE 1966, pp. 163-201.

66. Halajian, J.: Vehicle-Soil Mechanics on the Moon. Paper No. 63213 presented at the Automotive Engineering Congress, January 1963.

67. Anon: A Study of Lunar Traverse Missions. Jet Propulsion Lab. Document 760-26, Sept 16, 1968.

68. Karafiath, L. L.; and Nowatski, E. A.: A Study of the Effect of Sloping Ground on Bearing Strength and the Landing Performance of Space Vehicles. Grumman Research Dept. Memorandum RM-407, March 1968.

69. Ballinger, J. C.; and Christensen, E. H.: Environmental Control Study of Space Vehicles. General Dynamics, Convair Research Program No. 111-9121, Jan. 20, 1961.

70. Lyot, B.; Ann. Obs. Meudon, 8, 1929; also in Tech. Transl. F-187 (NASA, Washington, D. C., 1964); Dollfuss, A.; Ann. Astrophys. vol 19, no 71, 1956.

APPENDIX A
List of Symbols

a_1, a_2, a_3	parameters in brightness temperature equation (watts/m^2 – steradian)
a_4	parameter in brightness temperature equation (dimensionless)
A_n, B_n	Fourier coefficients in surface temperature equation (°K)
B	luminance, (candles/unit area)
c	specific heat (cal/gm°K)
D	block or crater diameter (meters)
E	solar constant, (lumens/unit area)
f	surface wave frequency (cycles/meter)
g	phase angle, angle between incident and reflected light, figure 15, (deg)
$g, i, \epsilon, \phi_i, \phi_\epsilon$	angles defined in figure 13 (deg)
I_o	infrared radiance (watt/m^2 – steradian)
I_1	intensity component of light vibration perpendicular to phase angle (candles)
I_2	intensity component of light vibration in the phase plane (candles)
k	thermal conductivity (watt/cm°K)
k_1	reflectivity (watt/cm°K $^{1/4}$)
k_o	conductivity constant (watt/cm°K)
K	exponent in mean slope equation
ΔL	lunar surface base length (meters)
n	coefficient in center frequency equation
N_o	cumulative frequency distribution of blocks or craters larger than diameter D (number/square meter)

P	lunation period (360°)
P_I	degree of polarization = $(I_1 - I_2)/(I_1 + I_2)$ (nondimensional)
t	time angle (deg)
T	surface temperature (°K)
T_E	equatorial brightness temperature (°K)
a	local lunar slope (deg) or, auxiliary angle for defining location of luminance meridian, figure 15 (deg)
$\overline{a}$	mean lunar slope (deg)
β	latitude (deg)
γ	thermal inertia parameter ($cm^2 sec^{1/2}$ °K/cal)
ϵ	dielectric constant (dimensionless)
λ	wavelength (meters)
$\xi(\lambda)$	wavelength dependent parameter (cm^3/gm)
σ	Stefan-Boltzman constant = 5.74×10^{-8} watts/m^2 $(°K)^4$
ρ	soil density (gm/cm^3) or, radiance factor (nondimensional)
ρ_o	normal albedo (nondimensional)
$\phi(g, a)$	photometric function (nondimensional)
$\tan \phi$	loss tangent (nondimensional)

APPENDIX B

Short Table of Conversion Factors

Multiply	By	To Obtain
m	3.281	ft
micron	3.281×10^{-6}	ft
angstrom	10^{-10}	m
km/sec	3281	ft/sec
m/sec^2	3.281	ft/sec^2
cycles/m	0.3048	cycles/ft
m^3/cycle	35.32	ft^3/cycle
gm/cm^3	1.940	$slugs/ft^3$
N	0.2248	lbf
N/cm^2	1.451	lbf/in^2
N/cm^3	3.687	lbf/in^3
joules	0.95×10^{-3}	BTU
watts	0.95×10^{-3}	BTU/sec
watts	1.00	joules/sec

APPENDIX C
Glossary

Angle of repose – The angle from the horizontal of the natural slope of the surface of a conical pile of material formed by dry-sifting the material onto a flat surface.

Antisolar point – The point on the Moon farthest from the Sun where the line joining the centers of the Sun and Moon intersect the lunar surface.

Brightness surge – Rapid increase in brightness near zero phase – radiance approximately doubles between 5 and 0 degrees phase angles.

Brightness temperature – Temperature of a black body computed from the Planck equation which gives off the same radiant power at the particular wave length. In this monograph, brightness temperature and infrared temperature are equivalent.

Dielectric constant – The ratio of the permittivity (ϵ) of a material to its free space value (ϵ_0). This ratio "k" is normally referred to as relative or effective dielectric constant.

Effective friction coefficient – Ratio between normal and horizontal force of footpad and lunar surface. Actual horizonal force includes both a friction and plowing action through the soil. Tabulated range is representative of the effective ratio estimated from Surveyor lunar landings and from the motion of the alpha scattering instrument package during the Surveyor 3 vernier engine firing experiment.

Geometric albedo – The brightness of the surface divided by the brightness of a Lambert surface having the same inclination as the surface. (Since the reflectivity of the moon appears to be independent of the incident and emergent angles at zero phase angle, the geometric albedo at zero phase angle can be considered equal to the normal albedo, even though their formal definitions only coincide at the sub-Earth point.)

Isophote – A line of equal or constant brightness.

Loss tangent – The capacity of a material to transmit a wave. Penetration depth increases with a decreasing value of the loss tangent.

Lunation – The average period of revolution of the Moon about the Earth with respect to the Sun, a period of 29 days, 12 hours, 44 minutes, 2.8 seconds.

Normal albedo – The brightness of the surface divided by the brightness of a Lambert surface (white screen) when observer and illuminator are located along the same normal vector.

Photoclinometry – The process of relating the measured brightness seen in a photograph, the viewing and lighting geometry, and the surface photometric function to obtain slope information.

Relief – Total vertical rise of a surface feature (i.e., bottom of crater to top of rim).

Rim height – Height of crater rim above local surface plane.

Sub-Earth point – The point on the lunar surface nearest to Earth where the line joining the centers of the Moon and Earth intersect the lunar surface.

Subsolar point – The point on the Moon where the Sun is at zenith.

Steradian – Solid angle subtended at the center of a sphere by an area on the surface equal to the square of the radius of the sphere. (The total solid angle about a point is 4π steradians.)

Terminator – The line that separates the illuminated and unilluminated portions of the moon.

Thermal inertia – A measure of the resistivity or resistance of a material to a change in temperature. The larger the value of the thermal inertia parameter, γ, the better the material acts as a thermal insulator.

Photometric function – The function relating reflectance properties of the surface to the viewing direction, solar illumination direction, and surface orientation.

Radiance factor – Ratio of observed radiance of a point on the surface to the radiance of a white screen placed normal to the incident solar rays, $\rho_o \phi (g,\alpha)$.

Rille – Trench-like lunar surface depression.

Vesiculated – Small spherical cavities in molten rocks. These cavities are produced by bubbles of air or gas.

NASA SPACE VEHICLE DESIGN CRITERIA MONOGRAPHS ISSUED TO DATE

SP-8001 (Structures)	Buffeting During Launch and Exit, May 1964
SP-8002 (Structures)	Flight-Loads Measurements During Launch and Exit, December 1964
SP-8003 (Structures)	Flutter, Buzz, and Divergence, July 1964
SP-8004 (Structures)	Panel Flutter, May 1965
SP-8005 (Environment)	Solar Electromagnetic Radiation, June 1965
SP-8006 (Structures)	Local Steady Aerodynamic Loads During Launch and Exit, May 1965
SP-8007 (Structures)	Buckling of Thin-Walled Circular Cylinders, revised August 1968
SP-8008 (Structures)	Prelaunch Ground Wind Loads, November 1965
SP-8009 (Structures)	Propellent Slosh Loads, August 1968
SP-8010 (Environment)	Models of Mars Atmosphere (1967), May 1968
SP-8011 (Environment)	Models of Venus Atmosphere (1968), December 1968
SP-8012 (Structures)	Natural Vibration Modal Analyses, September 1968
SP-8013 (Environment)	Meteoroid Environment Model-1969 (Near-Earth to Lunar Surface), March 1969
SP-8014 (Structures)	Entry Thermal Protection, August 1968
SP-8015 (Guidance and Control)	Guidance and Navigation for Entry Vehicles, November 1968
SP-8016 (Guidance and Control)	Effects of Structural Flexibility on Spacecraft Control Systems, April 1969
SP-8017 (Environment)	Magnetic Fields-Earth and Extraterrestrial, March 1969
SP-8018 (Guidance and Control)	Spacecraft Magnetic Torques, March 1969
SP-8019 (Structures)	Buckling of Thin-Walled Truncated Cones, September 1968

NASA-Langley, 1969 —— 30